AN APPLICATION OF THE FINITE DIFFERENCES METHOD TO A DYNAMICAL INTERFACE PROBLEM

İzzet Onur AĞIROĞLU

October, 2004

An Application of the Finite Differences Method to a Dynamical Interface Problem

By
İzzet Onur AĞIROĞLU

A Dissertation Submitted to the
Graduate School in Partial Fulfillment of the
Requirements for the Degree of

MASTER OF SCIENCE

Department: Mathematics
Major : Mathematics

İzmir Institute of Technology
İzmir, Turkey

October, 2004

We approve the thesis of **İzzet Onur AĞIROĞLU**

Date of Signature

27.10.2004

Assist. Prof. Dr. Gamze TANOĞLU
Supervisor
Department of Mathematics

27.10.2004

Assist. Prof. Dr. Ali İhsan NESLİTÜRK
Co-Supervisor
Department of Mathematics

27.10.2004

Prof. Dr. Gökmen TAYFUR
Co-Supervisor
Department of Civil Engineering

27.10.2004

Prof. Dr. Oktay PASHAEV
Department of Mathematics

27.10.2004

Assist. Prof. Dr. H. Seçil ALTUNDAĞ ARTEM
Department of Mechanical Engineering

27.10.2004

Assist. Prof. Dr. Gamze TANOĞLU
Head of Department

ACKNOWLEDGMENTS

I would like to give my endless gratitude to my supervisor Asst. Prof. Dr. Gamze TANOĞLU for her valuable guidance, patience and smiling face throughout this thesis.

I am indebted to my office mates; Zeynep Nilhan GÜRKAN and Figen AKINCI for sparks and catching fires, respectively.

I would like to thank to 7525 for their sincere effort to convert my figures and friendship.

Special thanks go to Hakan "the Specialist" KUTUCU (as I promised) for technical support and help for writing this thesis in LaTeX.

Finally, I would like to thank to my parents for their support and patience.

ABSTRACT

A multiple-order-parameter model for $Cu-Au$ system on a face cubic centered lattice was recently developed in the presence of anisotropy. In that model, three order parameters (non-conserved) and one concentration order parameter (conserved), which has been taken as a constant, were considered. Later on, the model has been extended, so that, concentration has been taken as a variable. It has been seen that two models were in a good agreement near critical temperature since the non-conserved order parameter behaves like a constant near critical temperature in both models. Thus, we extended the first model to a dynamical diffuse interface model near critical temperature.

After writing the free energy of the system in terms of the order parameters, minimizing the energy with respect to the order parameters and Langevin equation yield the non-linear system of parabolic equations. The finite differences method was implemented to solve this non-linear system of parabolic equations. The forward difference discretization was applied for the first derivative of the solution with respect to time and centered difference discretization was applied for the second order derivative of the solution with respect to spatial variable. We obtained stability criteria and find the error bound. The orientation dependence profiles, variation of interfacial energy and the effect of the degree of the anisotropy on the width of the diffuse interface are simulated when the time evolves.

ÖZET

Son zamanlarda, yüzey merkezli kübik yapı üzerindeki anizotropik $Cu-Au$ sistemi için bir çoklu durum parametresi modeli gelistirilmişti. Modelde, üç durum parametresi (korunan) ve sabit alınmış bir konsantrasyon durum parametresi (korunmayan) ele alınmıştı. Daha sonra bu model, konsantrasyon durum parametresinin değişken alınması suretiyle genişletilmiştir. İlk modelin ve genişletilmiş modelin, korunmayan durum parametresinin sabit gibi davranmasından dolayı, kritik sıcaklıkta iyi bir uyum gösterdikleri gözlenmiştir. Bu çalışma kritik sıcaklıkta yapılmış ve çalışmada ilk model, dinamik bir arayüzey problemine genişletilmiştir.

Sistemin enerjisi durum parametrelerine bağlı olarak yazıldıktan sonra, enerjinin durum parametrelerine göre minimize edilmesi ve Langevin denklemleriyle, doğrusal olmayan parabolik denklem sistemi elde edilmiştir. Bu denklem sistemini çözmek için sisteme sonlu farklar yöntemi uygulanmıştır. İleri sonlu fark ayrıklaştırılması, çözümün zamana göre türevine; merkezi sonlu fark ayrıklaştırılması ise çözümün uzaysal değişkene göre ikinci türevine uygulanmıştır. Kararlılık şartları ve hata sınırları elde edilmiştir. Zaman ilerledikçe, yöne bağlı profiller, arayüzey enerjisinin değişimi ve anizotropi derecesinin yayılım arayüzeyinin genişliğine olan etkisi betimlenmiştir.

TABLE OF CONTENTS

LIST OF FIGURES

Chapter 1

INTRODUCTION

The phase field model has attracted many scientists due to its ability in describing the complex pattern formation in phase transitions such as dendrites. It is a useful method for realistic simulation of microstructural evolution involving diffusion, coarsening of dendrites and the curvature and kinetic effects on the moving solid-liquid interface. It is efficient, especially in numerical treatment, because all the governing equations are written in a unified form without distinguishing the interface from solid or from the liquid phase. In the model, the phase field, $\phi(x,t)$, characterizes the physical state of the system at each position and time: $\phi = 1$ for the solid, $\phi = 0$ for the liquid, and $0 < \phi < 1$ at the interface. The phase field variable, ϕ, changes steeply but smoothly at the solid-liquid interface region, which avoids direct tracking of the interface position. Therefore, the model can be generated as a type of a diffuse interface model, which assumes that the interface has a finite thickness and that physical properties of the system vary smoothly through the interface.

A diffuse interface model was first developed by Van der Walls [1], who considered fluid density as an order parameter. Thereafter, by the mid of 1980's, the diffuse interface model was applied to the equilibrium properties of the interface [2], antiphase boundary migration by curvature [3], and to the second order phase transitions [4], but not to the first order phase transitions. Langer [5] proposed that the diffuse interface model could be applied to solidification phenomena. By using a singular perturbation method, Caginalp [6] proved that the phase field model could be reduced to the Stephan problem in the limit that the thickness of the interface approaches zero. Kobayashi [7] studied the dendritic growth of a pure melt and Wheeler, McFadden and Boettinger [8] proposed the phase field model for isothermal solidification of a binary alloy. Warren and Boettinger [9] investigated the dendritic growth of a binary alloy with the model of Wheeler, McFadden and Boettinger's [8].

The phase field models mentioned above suffer from two limitations which

severely restrict their range of applications. The first limitation is that the models can not simulate the case where the kinetic undercooling is negligibly small compared to the curvature undercooling (local equilibrium condition) [10]. The second is that the temperature variation in the finite interface region is negligibly small compared to the interface kinetic undercooling [10]. This restricts the size of the calculation domain and makes the reliable simulation of dendritic growth possible only at a large undercooling [11]. Karma and Rappel [10, 12] relieved these limitations and showed that it is feasible to determine the parameters in the phase field model at the thin interface limit (finite interface thickness condition) for the solidification of a pure melt using the concept, that the temperature gradient in the thin interface region could be linearly approximated. Following the work of Karma and Rappel, Kim *et al* [13, 14] demonstrated that the parameters in the phase field model for solidification of binary alloys can be determined at the thin interface limit by linearly approximated chemical potentials in the thin interface region [15].

One method for treating diffuse interfaces is to use a free energy functional for the system based on continuum parameters, that are spatially varying. The functional is written as integral of the sum of two kinds of terms; bulk energies, that are multiple-well functions of these parameters, and gradient energies that are (generally quadratic) functions of the gradients of the order parameters. The gradient part is included by the free energy functional because the translation between two phases is smooth. Both terms contribute to the energy in the transition regions that separate bulk phases [16].

One can obtain the evolution equations by using the variational arguments on these free-energy functionals. When the free-energy functional involves a single non-conserved scalar-order parameter, the result is the Cahn-Allen [17, 18] equation which is second-order non-linear parabolic equation. For a single conserved order parameter, say composition, the result is the Cahn-Hillard equation [19, 20]. Solidification of a binary mixture has been studied by Caginalp *et al* [21]. Warren and Boettinger [22, 23] derived a phase field model for isothermal solidification of a binary alloy.

Braun *et al* [16], developed a model for a binary alloy with two species on a face-centered cubic (fcc) lattice [24]: the atoms occupy the corners and the faces as shown in Figure 1.1. It has been customary to describe the fcc structure by four interpenetrating simple cubic "sublattices". Each sublattice represents a distinguished site which is repeated periodically to make up a crystal. The four sublattices are equivalent by symmetry of the fcc lattice [25].

At high temperatures, either of the atoms can occupy any site, and the

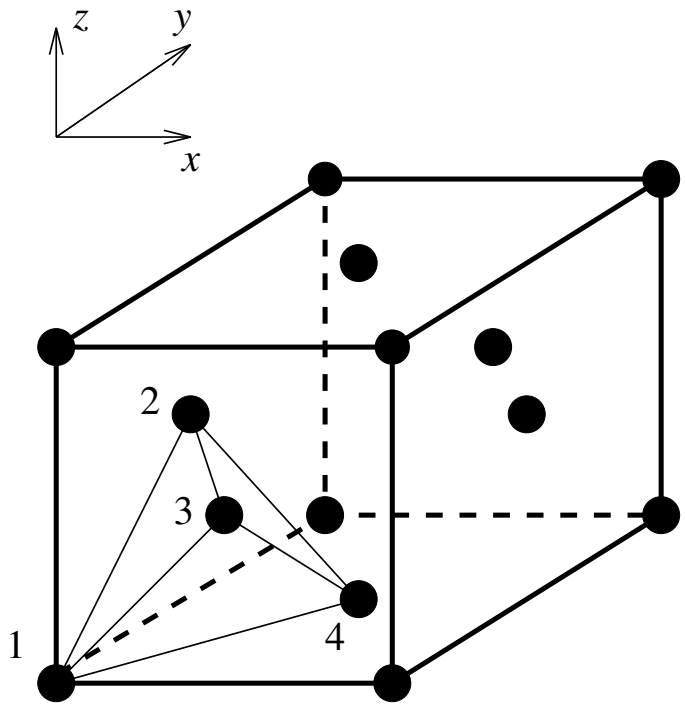

Figure 1.1: A schematic diagram of an fcc lattice. This lattice contains four interpenetrating simple cubic sublattices labelled by 1, 2, 3 and 4.

equilibrium state for this case is considered as disordered phase (with Strukturbericht notation $A1$ [26, 27]), which means the probabilities of finding either atom at each lattice point is equal. At low temperatures, ordered phases can be preferable. The ordered phases considered in this work are in the copper-gold ($Cu - Au$) system, where the corners of the lattice are different from the faces. The Cu_3Au phase with the copper atoms occupying the centers of the faces and the gold atoms at the corners is an example of $L1_2$ ordering in the Strukturbericht notation system. In this work, we consider $A1$ disordered phase and $L1_2$ ordered phase, and the structures we mentioned above are summarized in Figure 1.2 with their Strukturbericht notation [25].

In ordering of binary alloys on fcc lattices, one finds that not one but three(non-conserved) order parameters and an overall concentration(conserved order parameter) are required. The first model of ordering of a binary alloy on an fcc lattice for $Cu-Au$ system with gradient energy terms was developed by Braun *et al* [16] by using a multiple-order-parameter method. In that model, the overall concentration was taken constant through the interface; the focus was on the role played by three non-conserved order parameters in determining anisotropy of two types of boundaries; interphase boundaries (IPBs) and antiphase boundaries (APBs). The IPBs form between two different phases; they could be between two

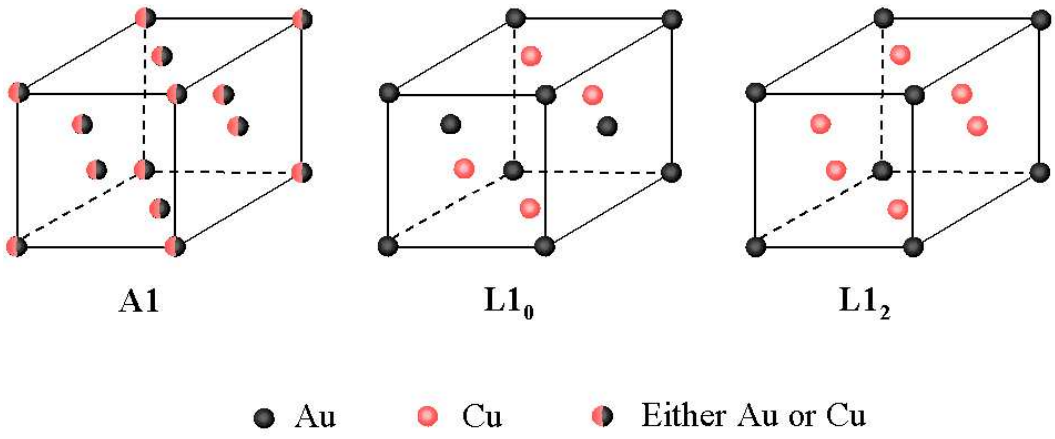

Figure 1.2: A schematic showing the Bulk phases for Binary Alloy on an fcc lattice. $A1$ represents the disordered state. Au and Cu atoms alternate for $L1_0$ structure. The corners are different from the faces for $L1_2$ structure.

different ordered phases or between an ordered and a disordered phase. APBs form between two domains of variants of the same phase(in this work we are not interested in APBs). In spite of that limitation, the model was successful in giving the anisotropy of IPBs between the disordered $A1$ phase and the ordered $L1_2$ phase [25]. But for an IPB, a uniform composition is inconsistent with the differences in the bulk concentrations in each phase at equilibrium. Moreover, for both APBs and IPBs, the assumption of a uniform composition leads to no adsorption, so that finding a temperature and composition-dependent interfacial free energy leads to a violation of the Gibbs adsorption equation [28]. For the interfacial energy anisotropy, IPBs were found to have relatively weak cubic anisotropy. The model also allowed a stable $L1_0$ phase. These different anisotropies occur naturally in the model once the form of the free energy is given. Furthermore, the dependence on orientation of properties of the interfaces is continuous and easily allows computation of the properties for all orientations. Lately, the previous model was generalized by G. Tanoglu [25] to the case where the concentration was free to vary through IPBs between ordered and disordered phases of a binary alloy on a lattice. The aim of that work was to compute phase boundaries at different places on the phase diagram for all orientations by using the extended model, and to show that above-mentioned success from the Braun's model still hold when the concentration varies through the IPB. In Braun's model, three non-conserved order parameters and one constant conserved order parameter were used. In the extended free energy model, the conserved order parameter was considered as a variable, to have a more realistic model. Thus, that the equations became more complex. In addition, the phase diagram of the $Cu - Au$ system was obtained

for the concentration $W < \frac{1}{2}$ and it's observed that the experimental and model phase diagram of $Cu - Au$ system are quite similar.

Many researchers have performed theoretical investigations on the diffusion-controlled phase transformation. Since the analytical solution of such problem is impossible, the recent remarkable developments in computers have made the numerical analysis of the non-linear diffusion equations possible, and computer simulations have become very useful for understanding the dynamics of phase transformation in materials. In the present thesis, we calculate the dynamics of microstructural changes in real alloys, i.e; $Cu - Au$ system, based on the multiple order parameter model developed by Braun *et al* [16]. We obtain interfacial properties of $Cu - Au$ system at equilibrium. Since we would like to understand phase-decomposition process, we extend the steady-state model to a non-steady dynamical problem. We only consider the phase-decomposition process at critical temperature (T_c), since the previous model is a good approximation of the extended model at the critical temperature, based on the numerical study of G.Tanoglu's thesis [25]. Their numerical simulations showed that the variation of concentration, W, is negligible, i.e; behaves like a constant, therefore, there is no need to include W as a parameter in the bulk free energy functional at T_c.

1.1 Outline

In this thesis, the numerical solution of the dynamical mathematical model which describes the ordering between the disordered phase $A1$ and ordered phase Cu_3Au for face-centered cubic alloy, based on the multiple order parameter model is studied. The finite difference method is implemented for this purpose.

In Chapter 2, the relation between the face-centered cubic lattice and order parameters is established. After introducing the free energy functional in terms of the order parameters, the bulk states are defined, and related to the free energy functional. Moreover, the system of non-linear parabolic equations are set up with the help of the Langevin Equation.

In Chapter 3, we briefly mention about the history of the explicit finite difference method. We then approximate the system of non-linear parabolic equations by explicit finite difference method. The stability criteria is obtained and error bound is found for the special orientation.

In Chapter 4, the dynamical process is exhibited for different orientations and different degrees of anisotropy. First, the behavior of the order parameters are simulated for different orientations. Then, the thickness of the interface is plotted for different orientations and degrees of anisotropy. The changing of the

interfacial energy with time is exhibited. We compare the exact solution with the numerical one in order to show the asymptotical stability of the method. Finally, we add the convection part to the diffusion-reaction equation, in order to obtain moving solution. We then solve this equation by finite difference method and exhibit the numerical results.

Chapter 2

FORMULATION

In this chapter, we begin with the relation between the fcc lattice and order parameters. Then we introduce the free energy of the system, $\mathcal{F}$, which is the integral of sum of two terms; bulk free energy and the gradient part. The relation between bulk free energy functional and bulk states is given. Finally, the system of parabolic equations are obtained by using Langevin and Euler-Ostrogradsky Equations.

An fcc crystal is a certain periodic arrangement of atoms, each associated with a point in a face-centered cubic Bravais lattice in 3-space. In Figure 2.1, we depict the unit cell of such a crystal. Each unit cell is occupied by four atoms, and so a tetrahedron can be associated to it. Each numbered point of such a tetrahedron can serve as the origin of a primitive cubic Bravais lattice. The fcc lattice is then decomposed into four numbered sublattices.

The example of alloy considered in this work is the Cu_3Au ordered structure, with the copper atoms occupying the centers of the faces and the gold atoms the vertices. Four numbers; $\rho_1, \rho_2, \rho_3,$ and ρ_4, are chosen as the corresponding fractional probability (when ordering is imperfect) densities of copper or gold on each primitive cubic sublattice are needed to describe this ordered structure. When ordering is perfect, copper represents $\frac{3}{4}$ of the total. Hence for the ordered Cu_3Au state

$$\rho_1(\text{ord}) = 0, \ \rho_2(\text{ord}) = \rho_3(\text{ord}) = \rho_4(\text{ord}) = 1 \tag{2.1}$$

while for the disordered fcc state

$$\rho_1(\text{dis}) = \rho_2(\text{dis}) = \rho_3(\text{dis}) = \rho_4(\text{dis}) = \frac{3}{4} \tag{2.2}$$

In our treatment the ρ's are taken to vary continuously and the specific problem we are addressing involves the transition between the disordered fcc and

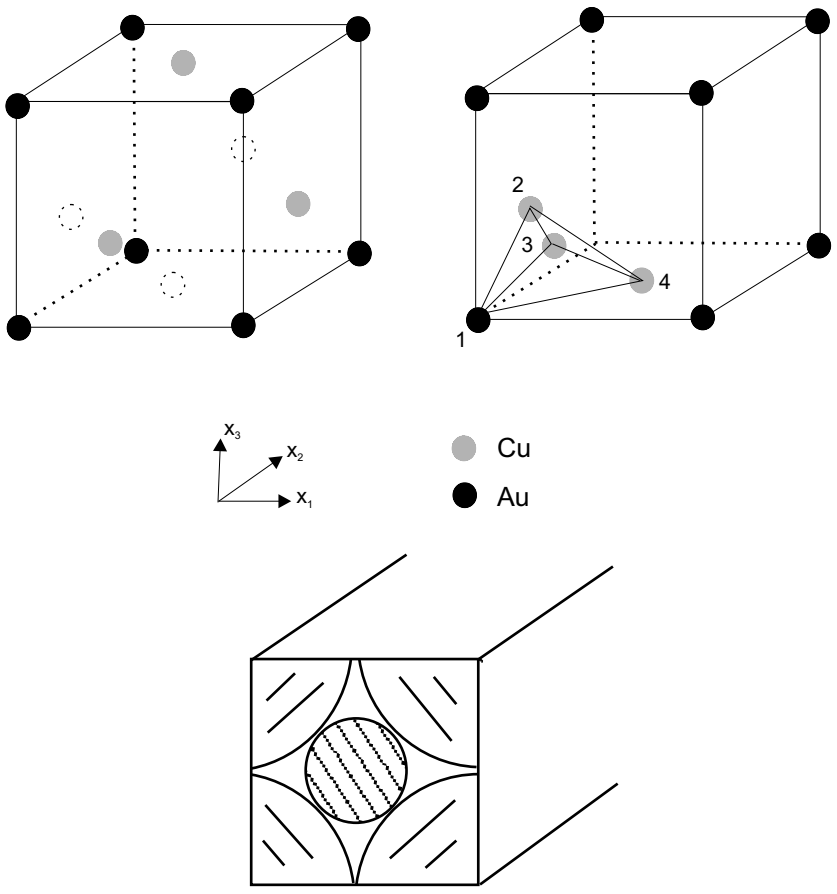

Figure 2.1: A unit cell of the fcc lattice, and the tetrahedron whose corners serves to number the four Primitive cubic sublattices. The Cu_3Au ordered structures arises when one of the sublattice, here labelled 1, has different occupation from the other three.

the ordered Cu_3Au state. The equations we will be dealing with are written in terms of the different variables X, Y, Z, W defined via

$$W = \frac{1}{4}(\rho_1 + \rho_2 + \rho_3 + \rho_4), \tag{2.3a}$$

$$X = \frac{1}{4}(\rho_1 + \rho_2 - \rho_3 - \rho_4), \tag{2.3b}$$

$$Y = \frac{1}{4}(\rho_1 - \rho_2 + \rho_3 - \rho_4), \tag{2.3c}$$

$$Z = \frac{1}{4}(\rho_1 - \rho_2 - \rho_3 + \rho_4) \tag{2.3d}$$

W represents the total relative density of copper in the system and in our treatment it will be taken fixed and equal to $\frac{3}{4}$, focusing our attention on the competition between different directions (anisotropy), ignoring the competition between different bulk states. In a more complete model W is taken not pointwise fixed, but only fixed on the average, see G. Tanoglu [25]. The ρ's can be recovered from X, Y, Z, W via

$$\rho_1 = W + X + Y + Z, \tag{2.4a}$$

$$\rho_2 = W + X - Y - Z, \tag{2.4b}$$

$$\rho_3 = W - X + Y - Z, \tag{2.4c}$$

$$\rho_4 = W - X - Y + Z \tag{2.4d}$$

The intuition behind the introduction of the new variables is that they are more amenable to continuizing [29]. In these variables, the disordered state corresponds to

$$X = 0,\ Y = 0,\ Z = 0 \tag{2.5}$$

and the ordered state to

$$X = -\frac{1}{4},\ Y = -\frac{1}{4},\ Z = -\frac{1}{4} \tag{2.6}$$

In what follows the variables are redefined as multiples by a fixed number of their previous meaning due to non-dimensionalization of the governing equations. To avoid another notation, we continue with X, Y, Z. In the new variables the *disordered state* is $X = 0, Y = 0, Z = 0$, while the *ordered state* is $X = 1, Y = 1, Z = 1$.

When W is held fixed, the free energy functional used in [16] is

$$\mathcal{F} = \int_V [\frac{1}{2}A(X_x^2 + Y_y^2 + Z_z^2) + \frac{1}{2}B(X_y^2 + X_z^2 + Y_x^2 + Y_z^2 + Z_x^2 + Z_y^2) + f(X, Y, Z)]dxdydz \tag{2.7}$$

where (x, y, z) are the space coordinates ranging in $V \subset I\!R^3$, and

$$\begin{aligned} f(X,Y,Z) &= a_2(X^2+Y^2+Z^2) + a_3\, XYZ \\ &\quad + a_{41}(X^4+Y^4+Z^4) + a_{42}(X^2Y^2+X^2Z^2+Y^2Z^2) \end{aligned} \tag{2.8}$$

with $a_2 = 2, a_3 = -12,\ a_{41} = a_{42} = 1$ and A, B independent constants. Other terms of the integral given in (2.7), i.e;

$$\frac{1}{2}A(X_x^2+Y_y^2+Z_z^2) + \frac{1}{2}B(X_y^2+X_z^2+Y_x^2+Y_z^2+Z_x^2+Z_y^2) \tag{2.9}$$

give the gradient part. We have the gradient part because the connection between two phases is smooth rather than sharp.

We refer to [16] for the derivation of the model and other relevant information. We only mention briefly that the form of f incorporates all the symmetries of the crystal. The cubic term is sufficient for the existence of first-order transitions and the associated interfaces [30]. The truncation to fourth order is discussed in Braun *et al* [16], and the extension to sixth order by [25]. The temperature enters through the coefficients. The form of the gradient part is derived so that the functional respects certain natural invariances and symmetries of fcc. The ratio $\frac{B}{A}$ measures the degree of anisotropy and it is the single most important parameter in our considerations.

The uniform equilibria are given as solutions to

$$f_X(X,Y,Z) = 2a_2X + a_3YZ + 4a_{41}X^3 + 2a_{42}X(Y^2+Z^2) = 0 \tag{2.10a}$$

$$f_Y(X,Y,Z) = 2a_2Y + a_3XZ + 4a_{41}Y^3 + 2a_{42}Y(X^2+Z^2) = 0 \tag{2.10b}$$

$$f_Z(X,Y,Z) = 2a_2Z + a_3XY + 4a_{41}Z^3 + 2a_{42}Z(X^2+Y^2) = 0 \tag{2.10c}$$

As can be seen, the order parameters, X, Y and Z are interchangeable $(X \leftrightarrow Y \leftrightarrow Z)$, and note that $(0,0,0)$ and $(1,1,1)$ satisfy

$$f(0,0,0) = f(1,1,1) = 0. \tag{2.11}$$

In order to derive a dynamical model, it is assumed that the system evolves in time so that its total free energy decreases monotonically. The evolution equation for the order parameters in the Ginzburg-Landau approach is the Langevin equation [15] which can be written as

$$\frac{\partial X_i}{\partial t} = -M\left(\frac{\delta \mathcal{F}}{\delta X_i}\right) \quad \text{where } X_1 = X, X_2 = Y, X_3 = Z \tag{2.12}$$

In this thesis, the mobility constant M is assumed as 1. The equation (2.7) can be written in the following form:

$$\mathcal{F} = \int_V H(X, Y, Z, X_x, X_y, X_z, Y_x, Y_y, Y_z, Z_x, Z_y, Z_z) dV \tag{2.13}$$

where

$$\begin{aligned} H = \frac{1}{2}A(X_x^2 + Y_y^2 + Z_z^2) &+ \frac{1}{2}B(X_y^2 + X_z^2 + Y_x^2 + Y_z^2 + Z_x^2 + Z_y^2) \\ &+ f(X, Y, Z) \end{aligned} \tag{2.14}$$

After applying the minimizing process, the variation of the free energy of the system with respect to the order parameters can be obtained from the Euler-Ostrogradsky equations [31]

$$\frac{\partial}{\partial x}H_{X_x} + \frac{\partial}{\partial y}H_{X_y} + \frac{\partial}{\partial z}H_{X_z} - H_X = X_t \tag{2.15a}$$

$$\frac{\partial}{\partial x}H_{Y_x} + \frac{\partial}{\partial y}H_{Y_y} + \frac{\partial}{\partial z}H_{Y_z} - H_Y = Y_t \tag{2.15b}$$

$$\frac{\partial}{\partial x}H_{Z_x} + \frac{\partial}{\partial y}H_{Z_y} + \frac{\partial}{\partial z}H_{Z_z} - H_Z = Z_t \tag{2.15c}$$

After using the explicit form of H given in (2.14), the equations (2.15) may be written as follows:

$$AX_{xx} + BX_{yy} + BX_{zz} - f_X = X_t \tag{2.16a}$$

$$BY_{xx} + AY_{yy} + BY_{zz} - f_Y = Y_t \tag{2.16b}$$

$$BZ_{xx} + BZ_{yy} + AZ_{zz} - f_Z = Z_t \tag{2.16c}$$

In these equations, the order parameters X, Y and Z depend on vector $\overrightarrow{x} = (x, y, z)$ and time t.

We shall consider the one dimensional solution of the governing equations (2.16), which represents a dynamical planar interfacial region separating an ordered $L1_2$ bulk phase from a disordered bulk phase at the same composition point. After defining the spatial variable ζ by

$$\zeta = \vec{n} \cdot \vec{x} = (n_x, n_y, n_z).(x, y, z) = xn_x + yn_y + zn_z \tag{2.17}$$

where $\vec{n} = (n_x, n_y, n_z)$ is the unit normal vector to the interface, the order parameters vary only in the direction parallel to the unit normal vector $\vec{n}$ to the interface. Now on, the new order parameters depend on a scalar, ζ, i.e;

$$X_i(\overrightarrow{x}) = \hat{X}_i(\overrightarrow{n}.\overrightarrow{x}) = \hat{X}_i(\zeta), \quad i = 1, 2, 3 \tag{2.18}$$

Applying the change of variable, the dependent variables become in the following form.

$$X_{xx} = n_x^2 \hat{X}_{\zeta\zeta}, \;\; X_{yy} = n_y^2 \hat{X}_{\zeta\zeta}, \;\; X_{zz} = n_z^2 \hat{X}_{\zeta\zeta} \tag{2.19a}$$

$$Y_{xx} = n_x^2 \hat{Y}_{\zeta\zeta}, \;\; Y_{yy} = n_y^2 \hat{Y}_{\zeta\zeta}, \;\; Y_{zz} = n_z^2 \hat{Y}_{\zeta\zeta} \tag{2.19b}$$

$$Z_{xx} = n_x^2 \hat{Z}_{\zeta\zeta}, \;\; Z_{yy} = n_y^2 \hat{Z}_{\zeta\zeta}, \;\; Z_{zz} = n_z^2 \hat{Z}_{\zeta\zeta} \tag{2.19c}$$

After substituting these expressions into equations (2.16) and collecting terms in the appropriate way, the governing equations reduce to the following system of non-linear parabolic differential equations.

$$\hat{X}_t = \lambda_x^2 \hat{X}_{\zeta\zeta} - f_{\hat{X}}(\hat{X}, \hat{Y}, \hat{Z}) \tag{2.20a}$$

$$\hat{Y}_t = \lambda_y^2 \hat{Y}_{\zeta\zeta} - f_{\hat{Y}}(\hat{X}, \hat{Y}, \hat{Z}) \tag{2.20b}$$

$$\hat{Z}_t = \lambda_z^2 \hat{Z}_{\zeta\zeta} - f_{\hat{Z}}(\hat{X}, \hat{Y}, \hat{Z}) \tag{2.20c}$$

The coefficients of the second derivatives which are given in (2.21) depend on the degree of anisotropy, $\epsilon^2 = B/A$, and orientations, prescribed with the components of the unit normal vector.

$$\lambda_x^2 = {n_x}^2 + \epsilon^2 {n_y}^2 + \epsilon^2 n_z^2 \tag{2.21a}$$

$$\lambda_y^2 = \epsilon^2 {n_x}^2 + {n_y}^2 + \epsilon^2 {n_z}^2 \tag{2.21b}$$

$$\lambda_z^2 = \epsilon^2 n_x^2 + \epsilon^2 n_y^2 + {n_z}^2 \tag{2.21c}$$

For simplicity, we will use the expressions without ($\hat{}$). After finding the first derivatives of the free energy functional with respect to the order parameters and substituting them, we rewrite the equations (2.20) as follows

$$X_t = \lambda_x^2 X_{\zeta\zeta} - (2a_2 X + a_3 YZ + 4a_{41} X^3 + 2a_{42} X(Y^2 + Z^2)) \tag{2.22a}$$

$$Y_t = \lambda_y^2 Y_{\zeta\zeta} - (2a_2 Y + a_3 XZ + 4a_{41} Y^3 + 2a_{42} Y(X^2 + Z^2)) \tag{2.22b}$$

$$Z_t = \lambda_z^2 Z_{\zeta\zeta} - (2a_2 Z + a_3 XY + 4a_{41} Z^3 + 2a_{42} Z(X^2 + Y^2)) \tag{2.22c}$$

The detailed derivation of this non-dimensionalization process is given in paper [16].

In order to solve this non-linear parabolic equations, we need to set up the boundary conditions and initial conditions. Since we are interested in the interface between $A1$ and $L1_2$ phases, left boundary conditions are

$$\lim_{\zeta \to -\infty} X(\zeta, t) = \lim_{\zeta \to -\infty} Y(\zeta, t) = \lim_{\zeta \to -\infty} Z(\zeta, t) = 0 \tag{2.23}$$

and right ones are

$$\lim_{\zeta \to \infty} X(\zeta, t) = \lim_{\zeta \to \infty} Y(\zeta, t) = \lim_{\zeta \to \infty} Z(\zeta, t) = 1 \tag{2.24}$$

We use the following step function for initial condition in our problem, since the thickness of the interface is 0 at $t = 0$.

$$X(\zeta, 0) = Y(\zeta, 0) = Z(\zeta, 0) = \begin{cases} 1 & \zeta \geq 0 \\ 0 & \zeta < 0 \end{cases} \tag{2.25}$$

2.1 Orientation Dependent Solution

We are interested in finding the orientation dependent interfacial properties of the interface between disordered phase $A1$ and the ordered phase Cu_3Au. The functional $f(X, Y, Z)$ is invariant to cyclic permutations of three variables, X, Y and Z for [111] orientation, and the boundary and initial conditions are the same for all order parameters. Thus, the number of equations in (2.22) can be reducible. But, for orientations that satisfy $\lambda_x^2 \neq \lambda_y^2 \neq \lambda_z^2$, the equations of motion are not invariant under permutation $X \leftrightarrow Y \leftrightarrow Z$.

This mathematical model allows us to simulate the structure of the interface for arbitrary orientation. When we change the orientation, the coefficients of the second derivatives in the equation (2.22) also change. Thus, we obtain different solutions of the system of equations for each orientation. The orientations are prescribed with two angles θ, the azimuthal angle, and ϕ, the polar angle. The Figure 2.2 shows these angles.

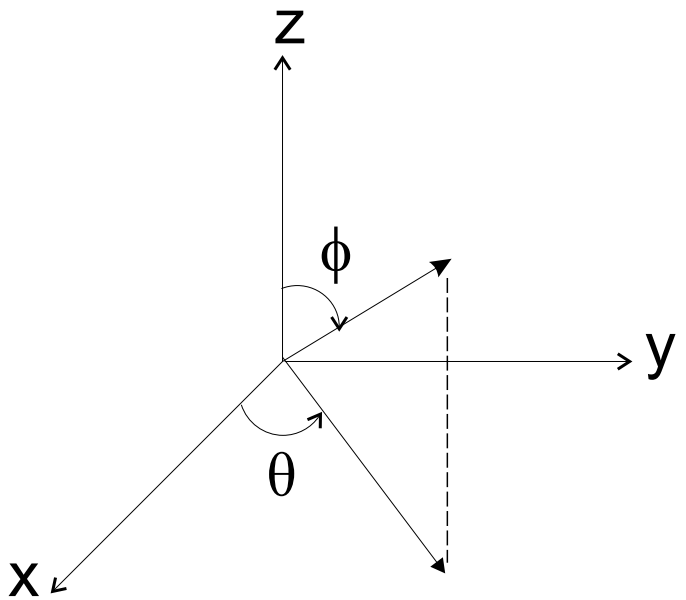

Figure 2.2: The azimuthal angle θ and polar angle ϕ.

The components of the unit normal vector in spherical coordinates may be written in terms of these angles.

$$n_x = \sin\phi\cos\theta \tag{2.26a}$$
$$n_y = \sin\phi\sin\theta \tag{2.26b}$$
$$n_z = \cos\phi \tag{2.26c}$$

One can easily show that

$$\begin{aligned} n_x^2 + n_y^2 + n_z^2 &= \sin^2\phi\cos^2\theta + \sin^2\phi\sin^2\theta + \cos^2\phi \\ &= \sin^2\phi(\cos^2\theta + \sin^2\theta) + \cos^2\phi \\ &= \sin^2\phi + \cos^2\phi \\ &= 1 \end{aligned}$$

In our study, we can compute the interfacial properties for arbitrary orientation by using the spherical coordinates of the unit normal vector. Now, we give examples for reduction of the number of the equations in the system.

For [a00] orientation ($\forall\ a \neq 0$), the components of the unit normal vector are $n_x = 1, n_y = n_z = 0$, and by using (2.21), we have $\lambda_x^2 = 1, \lambda_y^2 = \lambda_z^2 = \epsilon^2$, i.e; $Y \leftrightarrow Z$. So, (2.22), which contains three equations, reduces to a system with two equations

$$X_t = \lambda_x^2 X_{\zeta\zeta} - (2a_2X + a_3YZ + 4a_{41}X^3 + 2a_{42}X(Y^2 + Z^2)) \tag{2.27a}$$
$$Y_t = \lambda_y^2 Y_{\zeta\zeta} - (2a_2Y + a_3XZ + 4a_{41}Y^3 + 2a_{42}Y(X^2 + Z^2)) \tag{2.27b}$$

For orientation [aaa], ($\forall\ a \neq 0$), unit normal vector to the interface is $\vec{n} = (\frac{1}{\sqrt{3}}, \frac{1}{\sqrt{3}}, \frac{1}{\sqrt{3}})$, and $\lambda_x^2 = \lambda_y^2 = \lambda_z^2 = \lambda^2 = \frac{1}{3}(1 + 2\epsilon^2)$. So, our system (2.22) becomes

$$X_t = \lambda^2 X_{\zeta\zeta} - 4a_2X(X-1)(X - \frac{1}{2}) \tag{2.28}$$

by using the interchangeability of X, Y and Z.

Chapter 3

METHOD OF SOLVING

In this chapter, first we give the brief introduction about the history of the finite difference method. Then we obtain the finite difference approximation of the non-linear system of parabolic partial differential equations. Finally, we discuss stability and find the error bound.

3.1 Background for Finite Difference Method

We start with the fundamental theoretical paper by Courant, Friedrichs and Lewy [32], on the solutions of problems of mathematical physics by means of finite differences. In this paper, a discrete analogue of Dirichlet's principle was used to define an approximate solution by means of the five point approximation of Laplace's equation, and convergence as the mesh width tends to zero was established by compactness. A finite difference approximation was also defined for the wave equation. With its use of a variational principle for discretization and its discovery of the importance of mesh-ratio conditions in approximation of time-dependent problems this paper points forward and has had a great influence on numerical analysis of partial differential equations.

For time-dependent problems, considerable progress in finite difference methods was made during the period of the Second World War, when large-scale practical applications became possible with the aid of computers. A major role was played by the work of von Neumann, partly reported in O'Brien, Hyman and Kaplan [33]. For parabolic equations, a highlight of the early theory was the important paper by John [34]. For mixed initial-boundary value problems, the use of implicit methods was also established in this period by, e.g., Crank and Nicolson [35]. The finite difference theory for general initial value problems and parabolic problems then had an intense period of development during 1950s and 1960s, when the concept of stability was explored in the Lax equivalence

theorem and the Kreiss matrix lemmas, with further major contributions given by Douglas, Lees, Samarskii, Windlund and others.

Standart references on finite difference methods are the textbooks of Collatz [36], Forsythe and Wasow [37] and Richtmyer and Morton [38].

3.2 Application of the Explicit Finite Difference Method

In this thesis, the explicit finite difference method is implemented to solve the following system of non-linear parabolic equations which is obtained in the previous chapter and given in (2.22).

$$\begin{aligned} X_t &= \lambda_x^2 X_{\zeta\zeta} - (2a_2 X + a_3 YZ + 4a_{41}X^3 + 2a_{42}X(Y^2+Z^2)) \\ Y_t &= \lambda_y^2 Y_{\zeta\zeta} - (2a_2 Y + a_3 XZ + 4a_{41}Y^3 + 2a_{42}Y(X^2+Z^2)) \\ Z_t &= \lambda_z^2 Z_{\zeta\zeta} - (2a_2 Z + a_3 XY + 4a_{41}Z^3 + 2a_{42}Z(X^2+Y^2)) \end{aligned}$$

with constants $a_2 = 2, a_3 = -12,\ a_{41} = a_{42} = 1$. For this purpose, the FORTRAN code which is given in the appendix is implemented.

In order to approximate system (2.22) by finite difference method, we divide the closed domain by a set of lines parallel to the x- and t-axis to form a grid or mesh. We shall assume that the sets of lines are equally spaced. The domain is restricted on $[-L, L]$ and the finite time interval is considered as [0,T], for fixed T.

We denote the discrete approximation $X(\zeta_i, t_n)$ as X_i^n where

$$\zeta_i = -L + i\Delta\zeta,\ \ (i = 0, 1, ..., N_\zeta),\ \text{ and }\ \Delta\zeta = \frac{2L}{N_\zeta} \tag{3.2}$$

and

$$t_n = n\Delta t,\ \ (n = 0, ..., T/\Delta t) \tag{3.3}$$

We use the forward difference approximation for the time derivatives

$$(X_t)_i^n = \frac{X_i^{n+1} - X_i^n}{\Delta t} + O(\Delta t) \tag{3.4a}$$

$$(Y_t)_i^n = \frac{Y_i^{n+1} - Y_i^n}{\Delta t} + O(\Delta t) \tag{3.4b}$$

$$(Z_t)_i^n = \frac{Z_i^{n+1} - Z_i^n}{\Delta t} + O(\Delta t) \tag{3.4c}$$

and centered second difference approximation for the second order space derivatives

$$(X_{\zeta\zeta})_i^n = \frac{X_{i+1}^n - 2X_i^n + X_{i-1}^n}{(\Delta\zeta)^2} + O((\Delta\zeta)^2) \tag{3.5a}$$

$$(Y_{\zeta\zeta})_i^n = \frac{Y_{i+1}^n - 2Y_i^n + Y_{i-1}^n}{(\Delta\zeta)^2} + O((\Delta\zeta)^2) \tag{3.5b}$$

$$(Z_{\zeta\zeta})_i^n = \frac{Z_{i+1}^n - 2Z_i^n + Z_{i-1}^n}{(\Delta\zeta)^2} + O((\Delta\zeta)^2) \tag{3.5c}$$

We then substitute the approximations (3.4) and (3.5) into the system of equations (2.22). The one-step explicit finite difference approximations of the equations (2.22) are given in equation (3.6)

$$\begin{aligned} X_i^{n+1} &\approx \frac{\lambda_x^2 \Delta t}{(\Delta\zeta)^2}(X_{i+1}^n - 2X_i^n + X_{i-1}^n) \qquad (3.6a)\\ &\quad -(2a_2 X_i^n + a_3 Y_i^n Z_i^n + 4a_{41}(X_i^n)^3 + 2a_{42} X_i^n((Y_i^n)^2 + (Z_i^n)^2))\Delta t + X_i^n \\ Y_i^{n+1} &\approx \frac{\lambda_y^2 \Delta t}{(\Delta\zeta)^2}(Y_{i+1}^n - 2Y_i^n + Y_{i-1}^n) \qquad (3.6b)\\ &\quad -(2a_2 Y_i^n + a_3 X_i^n Z_i^n + 4a_{41}(Y_i^n)^3 + 2a_{42} Y_i^n((X_i^n)^2 + (Z_i^n)^2))\Delta t + Y_i^n \\ Z_i^{n+1} &\approx \frac{\lambda_z^2 \Delta t}{(\Delta\zeta)^2}(Z_{i+1}^n - 2Z_i^n + Z_{i-1}^n) \qquad (3.6c)\\ &\quad -(2a_2 Z_i^n + a_3 X_i^n Y_i^n + 4a_{41}(Z_i^n)^3 + 2a_{42} Z_i^n((X_i^n)^2 + (Y_i^n)^2))\Delta t + Z_i^n \end{aligned}$$

Thus, the order of the convergence of the method is $O(\Delta t) + O((\Delta\zeta)^2)$.

The schematic diagram summarizes the solution method in Figure 3.1. In the figure, boundary conditions for space variables (see equations (2.23) and (2.24)), and initial condition for time variables are known (see equation (2.25)). Intersection points of the lines parallel to the x- and t-axis are shown as dots. Because of the centered approximation for space variable, we have to use three points, denoted by $i-1,\ i,\ i+1$, in order to go one step up.

3.3 Stability and Error Analysis

In this section, we establish the stability criteria and error bound. We prove the lemma which states the stability criteria for [111] equation and we show that error is bounded.

3.3.1 Stability

A method is said to be stable if a small deviation from the true solution does not tend to grow as the solution is iterated.

We are interested in establishing the stability criteria for non-linear diffusion-reaction equation for the special case, [111] orientation. Because of the form of the free energy functional, the stability criteria for [111] orientation is valid for all orientations. More detailed study can be deduced as a future work.

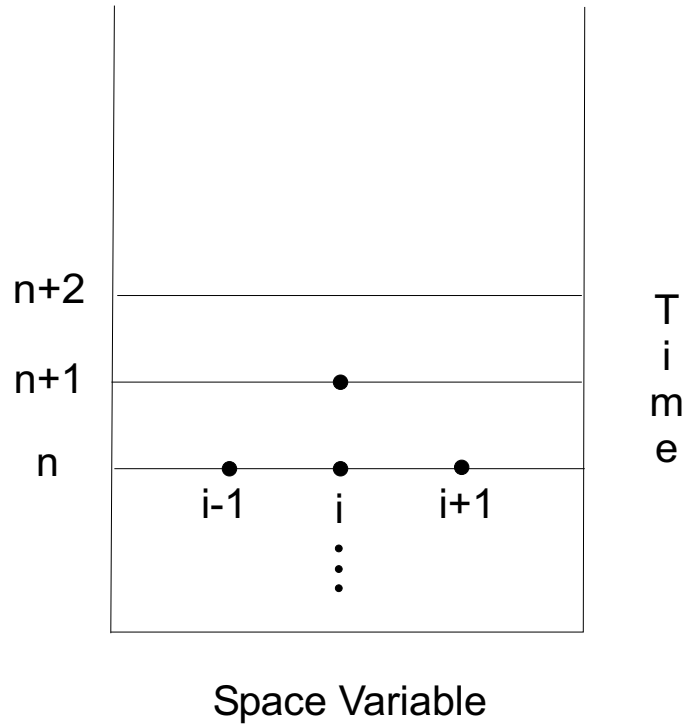

Figure 3.1: Schematic diagram for finite difference approximation.

We state and prove the stability criteria, i.e; the relation between $\Delta\zeta$ and Δt for the scheme, for the equation (2.28). Note that since $a_2 = 2$, equation (2.28) becomes

$$X_t = \lambda^2 X_{\zeta\zeta} - 8X(X-1)(X-\frac{1}{2}) \tag{3.7}$$

The Lax-Richtmyer Equivalence Theorem [40], which is given in Theorem 1, is the fundamental theorem for the finite difference schemes for the initial value problems. Theorem 1 states the relation between convergency and stability.

Theorem 1. (The Lax-Richtmyer Equivalence Theorem)

A consistent finite difference scheme for a partial differential equation for which the initial value problem is well-posed is convergent if and only if it is stable.

We establish the following stability criteria for [111] equation in Lemma 1.

Lemma 1. (The stability criteria)

The stability condition for the explicit method for the [111] orientation is

$$\Delta t \leq \frac{1}{\frac{2\lambda^2}{(\Delta\zeta)^2} + \max|a'(\eta)|} \tag{3.8}$$

where

$$a(\eta) = 8\eta(\eta - 1)(\eta - \frac{1}{2}) \tag{3.9}$$

Proof:

Let u_i^n represent the exact solution and U_i^n represent the numerical approximation. After substituting these expression into equation (3.7), we get the following equations:

$$U_i^{n+1} = \lambda^2\nu(U_{i+1}^n - 2U_i^n + U_{i-1}^n) - 8\Delta t U_i^n(U_i^n - 1)(U_i^n - \frac{1}{2}) + U_i^n \tag{3.10}$$

$$u_i^{n+1} = \lambda^2\nu(u_{i+1}^n - 2u_i^n + u_{i-1}^n) - 8\Delta t u_i^n(u_i^n - 1)(u_i^n - \frac{1}{2}) + u_i^n + \Delta t T_i^n \tag{3.11}$$

where $\nu = \frac{\Delta t}{(\Delta\zeta)^2}$ and T_i^n is the truncation error.

Let e_i^n represents the discretization error which is the difference between the numerical approximation and exact solution, i.e;

$$e_i^n = U_i^n - u_i^n \tag{3.12}$$

After subtracting (3.11) from (3.10), we get the one-step iteration approximation for the error as follows

$$e_i^{n+1} = \lambda^2\nu(e_{i+1}^n - 2e_i^n + e_{i-1}^n) - \Delta t(a(U_i^n) - a(u_i^n)) + e_i^n - \Delta t T_i^n \tag{3.13}$$

First, we write the Taylor expansion of $a(u_i^n)$ near U_i^n in equation (3.14)

$$a(u_i^n) = a(U_i^n) + (u_i^n - U_i^n)\frac{a'(U_i^n)}{1!} + (u_i^n - U_i^n)^2\frac{a''(U_i^n)}{2!} + \ldots \tag{3.14}$$

and then we approximate this expansion linearly;

$$a(u_i^n) \approx a(U_i^n) - e_i^n a'(\eta) \tag{3.15}$$

where $u_i^n < \eta < U_i^n$.

By using approximation (3.15), equation (3.13) can be written in the following form

$$e_i^{n+1} \approx e_i^n(-2\lambda^2\nu - \Delta t a'(\eta) + 1) + \lambda^2\nu e_{i+1}^n + \lambda^2\nu e_{i-1}^n - \Delta t T_i^n \tag{3.16}$$

The Maximum Principle tells us that the coefficients of e_i^n, e_{i+1}^n and e_{i-1}^n must be equal or greater than zero [39]. Since the coefficients of e_{i+1}^n and e_{i-1}^n are positive, we only consider the coefficient of e_i^n.

$$-2\lambda^2\nu - \Delta t a'(\eta) + 1 \geq 0 \tag{3.17}$$

$$-2\lambda^2\frac{\Delta t}{(\Delta\zeta)^2} - \Delta t a'(\eta) + 1 \geq 0 \tag{3.18}$$

$$-\Delta t(\frac{2\lambda^2}{(\Delta\zeta)^2} + a'(\eta)) \geq -1 \tag{3.19}$$

$$\Delta t(\frac{2\lambda^2}{(\Delta\zeta)^2} + a'(\eta)) \leq 1 \tag{3.20}$$

Finally, the stability criteria for (3.7) is obtained as follows

$$\Delta t \leq \frac{1}{\frac{2\lambda^2}{(\Delta\zeta)^2} + \max|a'(\eta)|} \tag{3.21}$$

The graph of $a'(\eta)$ is given in Figure 3.2 and as it can be seen from the figure, the maximum value of $\max|a'(\eta)|$ is 4 for $0 \leq \eta \leq 1$.

In Figure 3.3, the relation between $\Delta\zeta$ and Δt is shown. The solid line is the equation of the curve

$$\Delta t = \frac{1}{\frac{2\lambda^2}{(\Delta\zeta)^2} + 4} \tag{3.22}$$

The stability region is the region below the solid line. We pick $\Delta\zeta = 0.05$ and $\Delta t = 0.001$ in our calculations to satisfy the stability criteria.

One of the property of the parabolic equations is

$$\sup_x |u(\zeta, t)| \leq \sup_x |u(\zeta, t')| \quad if \quad t > t'. \tag{3.23}$$

In order to observe that the numerical solution of [111] equation satisfies this property, we now plot the numerical solution as function of time. As can be seen in Figure 3.4, the numerical solution is decreasing as time evolves.

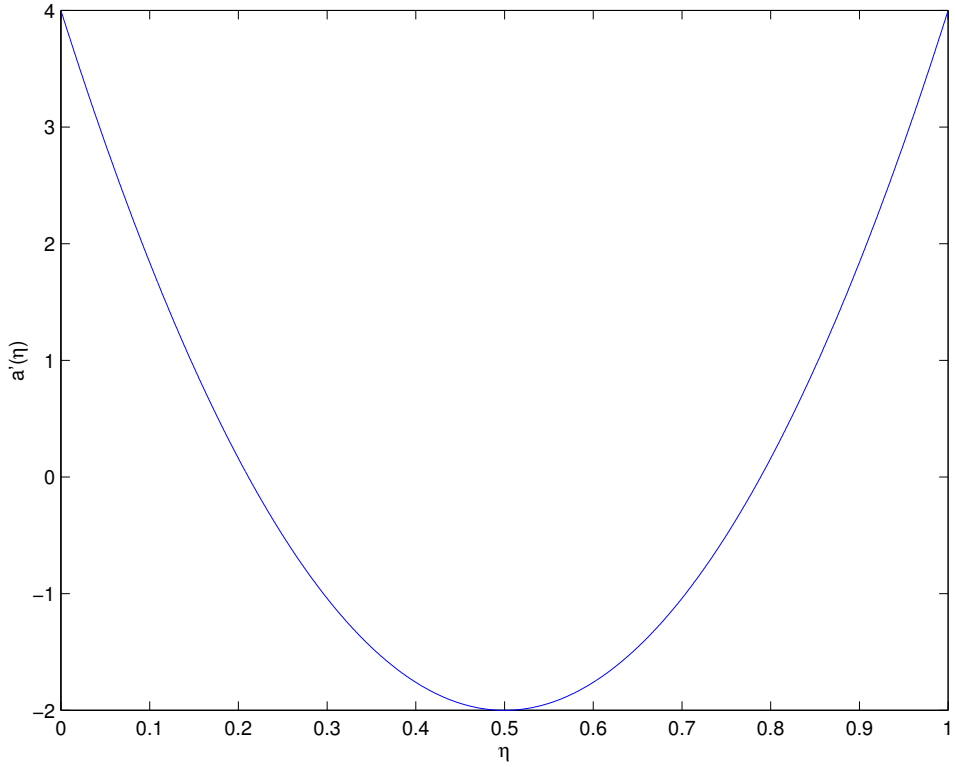

Figure 3.2: Graph of $a'(\eta)$

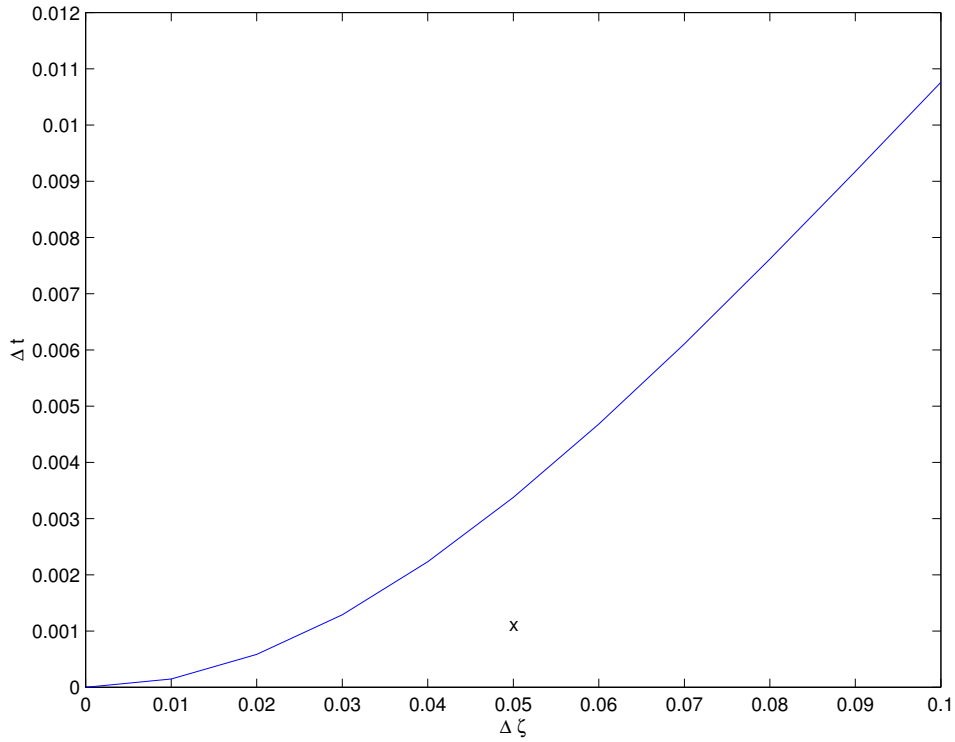

Figure 3.3: This figure shows the stability region for equation (3.7). Stability region is the region below the solid line.

Thus,

$$|U^{n+1}| < |U^n|, \tag{3.24}$$

where the norm we use is

$$|U^n| = \sum_{i=0}^{\infty} U_i^n. \tag{3.25}$$

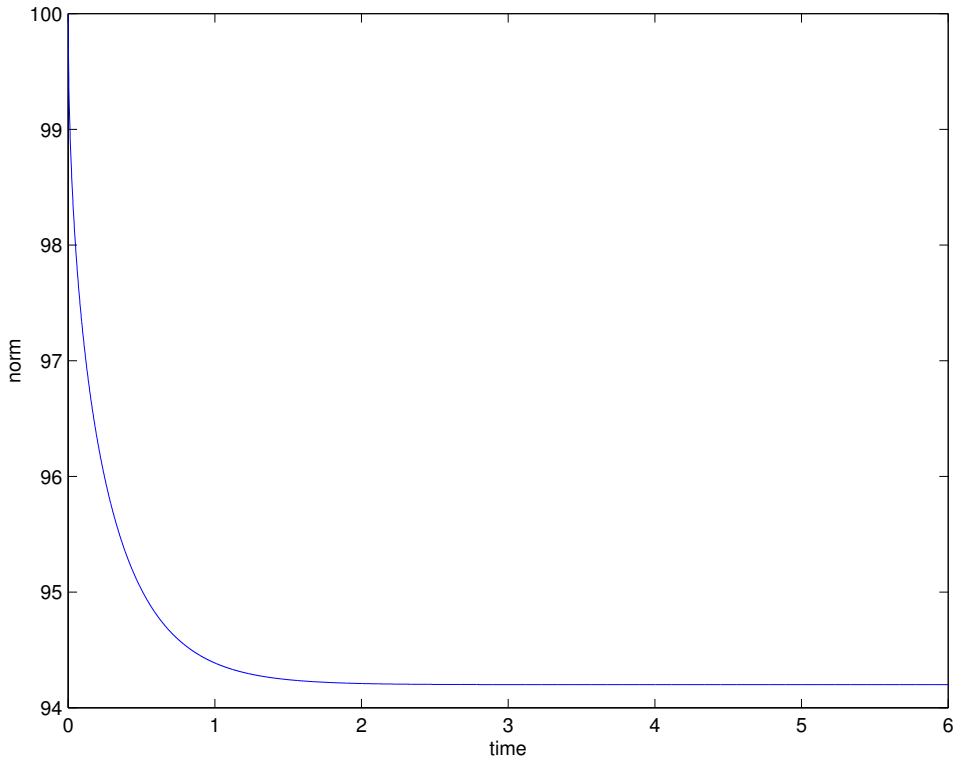

Figure 3.4: This figure simulates the sequence of the norm $|U^n|$ is decreasing, thus scheme is stable.

As a result, after stating the stability for criteria (3.8) and picking the values of $\Delta\zeta$ and Δt, (according to the Lax-Richtmyer Equivalence Theorem) we say that the scheme is convergent.

3.3.2 Asymptotical Stability

In this section, asymptotical stability is discussed. We start with giving the definition of asymptotical stability.

Definition 1.

Let $\widetilde{X}(\zeta)$ be the exact solution of equilibrium equation

$$\lambda^2 \widetilde{X}_{\zeta\zeta} = 4a_2 \widetilde{X}(\widetilde{X} - 1)(\widetilde{X} - \frac{1}{2}) \tag{3.26}$$

and X_i^n be the solution of time dependent non-linear parabolic equation (2.28). If the numerical solution X_i^n approaches the exact solution $\widetilde{X}(\zeta)$ when $t \to \infty$, it is said that the numerical solution is asymptotically stable.

Lemma 2.

The numerical solution of the problem for [111] orientation is asymptotically stable.

Proof:

First, we exactly solve the equilibrium equation (3.26). The equilibrium equation for [111] orientation is

$$\lambda^2 \widetilde{X}_{\zeta\zeta} = 4a_2(\widetilde{X}^3 - \frac{3}{2}\widetilde{X}^2 + \frac{1}{2}\widetilde{X}) \tag{3.27}$$

after multiplying the parenthesis at right hand side. Then, we multiply both sides by $\widetilde{X}_\zeta$ and get the equality

$$\lambda^2 \widetilde{X}_{\zeta\zeta}\widetilde{X}_\zeta = 4a_2(\widetilde{X}^3 - \frac{3}{2}\widetilde{X}^2 + \frac{1}{2})\widetilde{X}_\zeta \tag{3.28}$$

Since

$$\widetilde{X}_{\zeta\zeta}\widetilde{X}_\zeta = \frac{1}{2}\frac{d}{d\zeta}(\widetilde{X}_\zeta)^2 \tag{3.29}$$

we get the following form

$$\lambda^2 \frac{d}{d\zeta}(\widetilde{X}_\zeta)^2 = 8a_2(\widetilde{X}^3 - \frac{3}{2}\widetilde{X}^2 + \frac{1}{2})\widetilde{X}_\zeta \tag{3.30}$$

We write $\widetilde{X}_\zeta = \frac{d\widetilde{X}}{d\zeta}$ and take the integral of both sides

$$\lambda^2 \int \frac{d}{d\zeta}(\widetilde{X}_\zeta)^2 d\zeta = 8a_2 \int (\widetilde{X}^3 - \frac{3}{2}\widetilde{X}^2 + \frac{1}{2})d\widetilde{X} \tag{3.31}$$

or

$$\lambda^2(\widetilde{X}_\zeta)^2 = 8a_2(\frac{1}{4}\widetilde{X}^4 - \frac{1}{2}\widetilde{X}^3 + \frac{1}{4}\widetilde{X}^2) + c \tag{3.32}$$

Pick $c = 0$,

$$\lambda^2(\widetilde{X}_\zeta)^2 = 8a_2\frac{1}{4}\widetilde{X}^2(\widetilde{X}^2 - 2\widetilde{X} + 1) \tag{3.33}$$

$$\lambda^2(\widetilde{X}_\zeta)^2 = 2a_2\widetilde{X}^2(\widetilde{X}^2 - 2\widetilde{X} + 1) \tag{3.34}$$

$$(\widetilde{X}_\zeta)^2 = \frac{2a_2}{\lambda^2}\widetilde{X}^2(\widetilde{X}^2 - 2\widetilde{X} + 1) \tag{3.35}$$

$$(\widetilde{X}_\zeta)^2 = \frac{2a_2}{\lambda^2}\widetilde{X}^2(\widetilde{X}-1)^2 \tag{3.36}$$

Take the square root of both sides,

$$\sqrt{(\widetilde{X}_\zeta)^2} = \sqrt{\frac{2a_2}{\lambda^2}\widetilde{X}^2(\widetilde{X}-1)^2} \tag{3.37}$$

$$|\widetilde{X}_\zeta| = \frac{\sqrt{2a_2}}{|\lambda|}|\widetilde{X}(\widetilde{X}-1)| \tag{3.38}$$

Since $\lambda > 0$, $\widetilde{X}(\widetilde{X}-1) \leq 0$ for the interval $0 \leq \widetilde{X} \leq 1$, and $\widetilde{X}_\zeta > 0$,

$$\widetilde{X}_\zeta = -\frac{\sqrt{2a_2}}{\lambda}\widetilde{X}(\widetilde{X}-1) \tag{3.39}$$

or

$$\frac{d\widetilde{X}}{\widetilde{X}(\widetilde{X}-1)} = -\frac{\sqrt{2a_2}}{\lambda}d\zeta \tag{3.40}$$

Integrate both sides,

$$\ln|\widetilde{X}-1| - \ln|\widetilde{X}| = -\frac{\sqrt{2a_2}}{\lambda}\zeta + d \tag{3.41}$$

Pick $d = \frac{\sqrt{2a_2}}{\lambda}\zeta_0$

$$\ln|\frac{\widetilde{X}-1}{\widetilde{X}}| = -\frac{\sqrt{2a_2}}{\lambda}(\zeta-\zeta_0) \tag{3.42}$$

Since $\frac{\widetilde{X}-1}{\widetilde{X}} < 0$ in the interval $0 < \widetilde{X} < 1$,

$$\frac{1-\widetilde{X}}{\widetilde{X}} = \exp(-\frac{\sqrt{2a_2}(\zeta-\zeta_0)}{\lambda}) \tag{3.43}$$

thus,

$$\widetilde{X} = \frac{1}{1+\exp(-\frac{\sqrt{2a_2}(\zeta-\zeta_0)}{\lambda})} \tag{3.44}$$

Since

$$\frac{1}{2}(1+\tanh a) = \frac{1}{1+\exp(-2a)} \tag{3.45}$$

where

$$a = \frac{\sqrt{a_2}(\zeta-\zeta_0)}{\sqrt{2}\lambda} \tag{3.46}$$

the solution of the equation (3.26) becomes

$$\widetilde{X} = \frac{1}{2}(1+\tanh\frac{\sqrt{a_2}(\zeta-\zeta_0)}{\sqrt{2}\lambda}) \tag{3.47}$$

The solution (3.47) exhibits the translation invariance of the problem. For simplicity, we assume position $\zeta_0 = 0$.

Now, we simulate the comparison of the exact solution $\widetilde{X}$ (3.47) for equilibrium equation (3.26) to the numerical solution X_i^n of the equation for [111] orientation (2.28) when $t \to \infty$ in Figure 3.5. It is not possible for us to take t to infinity. We observe that the system reaches equilibrium at $t = 5$ and nothing changes for time $t > 5$. Thus, we simulate the solution for [111] orientation for $t = 5$ and the exact solution for equilibrium. As it can be seen, numerical solution is asymptotically stable.

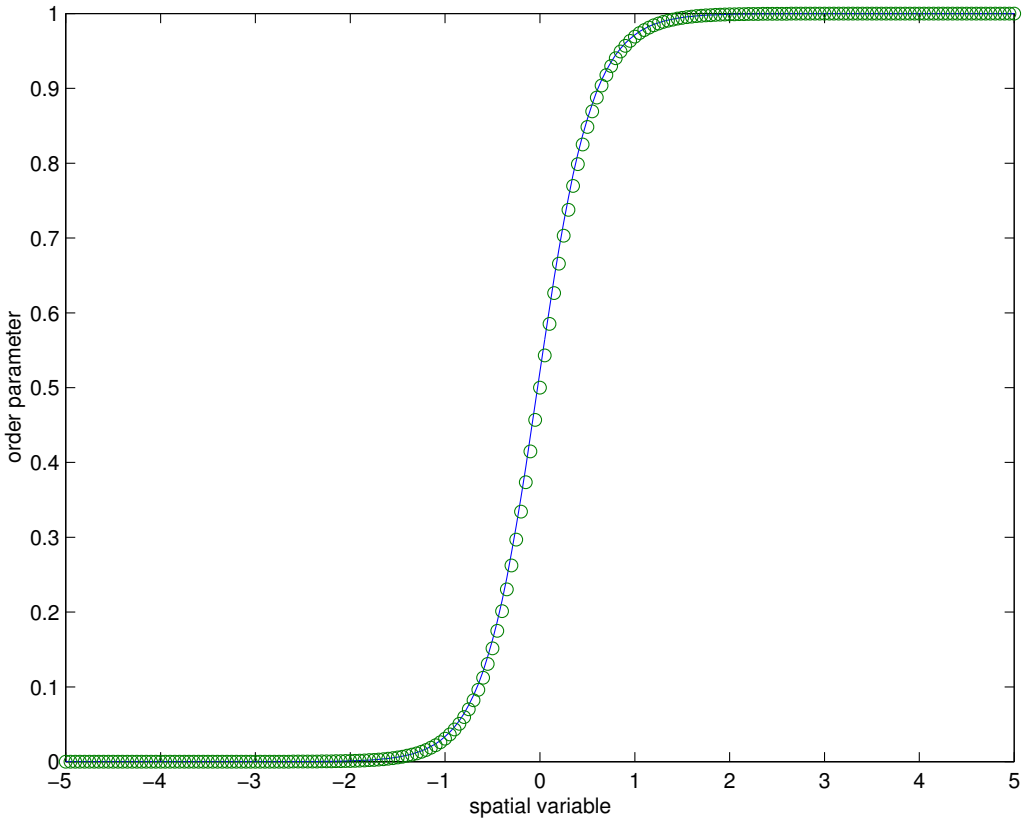

Figure 3.5: The numerical and exact solutions.

3.3.3 Error Analysis

The error of the numerical solution will tend to zero along the refinement path, as required, provided that the initial and boundary values are consistent; that is, the errors in the initial and boundary values also tend to zero along the refinement path. But, for the non-linear problem, we are expecting to see the error bound is small. In this section, we find the error bound for [111] equation.

Lemma 3. (Error Bound for [111] Orientation)

The error bound for the scheme for [111] equation is

$$0 \leq E^n \leq e^{-c+T}\hat{T}T \tag{3.48}$$

where c is the maximum value of $|a'(\zeta)|$ and $\hat{T} = \sum_i^\infty T_i^n$ with truncation error T_i^n.

Proof:

We start with equation (3.13) obtained in previous section

$$e_i^{n+1} = \lambda^2\nu(e_{i+1}^n - 2e_i^n + e_{i-1}^n) - \Delta t(a(U_i^n) - a(u_i^n)) + e_i^n - \Delta t T_i^n$$

Next, since $e_i^n \geq 0, \ \forall i, n$, we define E^n and $\hat{T}$ as

$$E^n = \sum_i^\infty e_i^n \ \text{ and } \ \hat{T} = \sum_i^\infty T_i^n \tag{3.49}$$

By using (3.15) and take the sum of both sides, we get the following equation

$$\sum_i^\infty e_i^{n+1} = \lambda^2\nu(\sum_i^\infty e_{i+1}^n - 2\sum_i^\infty e_i^n + \sum_i^\infty e_{i-1}^n) - \Delta t a'(\eta)\sum_i^\infty e_i^n + \sum_i^\infty e_i^n - \Delta t\sum_i^\infty T_i^n \tag{3.50}$$

Since

$$\sum_i^\infty e_{i-1}^n = \sum_i^\infty e_i^n = \sum_i^\infty e_{i+1}^n = E^n \tag{3.51}$$

we get

$$E^{n+1} \leq E^n(1 + c\Delta t) + \hat{T}\Delta t \tag{3.52}$$

For the zeroth step, there is no error, i.e; $E^0 = 0$

$$E^1 \leq \hat{T}\Delta t \tag{3.53}$$

$$E^2 \leq (1 + c\Delta t)\hat{T}\Delta t + \hat{T}\Delta t = [1 + (1 + c\Delta t)]\hat{T}\Delta t \tag{3.54}$$

$$E^3 \leq (1+c\Delta t)[1+(1+c\Delta t)]\hat{T}\Delta t+\hat{T}\Delta t = [1+(1+c\Delta t)+(1+c\Delta t)^2]\hat{T}\Delta t \tag{3.55}$$

$$\vdots$$

$$E^n \leq [1 + (1 + c\Delta t) + (1 + c\Delta t)^2 + \ldots + (1 + c\Delta t)^{n-1}]\hat{T}\Delta t \tag{3.56}$$

By using the property

$$(1+x)^n \leq e^{nx} \tag{3.57}$$

we get

$$E^n \leq [1 + e^{c\Delta t} + e^{2c\Delta t} + e^{3c\Delta t} + \ldots + e^{(n-1)c\Delta t}]\hat{T}\Delta t \tag{3.58}$$

Since

$$e^{c\Delta t} \leq e^{2c\Delta t} \leq e^{3c\Delta t} \leq \ldots \leq e^{(n-1)c\Delta t} \tag{3.59}$$

we get

$$E^n \leq ne^{(n-1)c\Delta t}\hat{T}\Delta t \tag{3.60}$$

Since $T = n\Delta t$ and $E^n \leq 0$, we get the boundary for error as following

$$0 \leq E^n \leq e^{-c+T}\hat{T}T \tag{3.61}$$

3.4 Computer Programming

We write a FORTRAN code to solve the finite difference equations (3.6). The program allows us to solve the system of parabolic equations (2.22), to find the thickness of the interface, to calculate the interfacial energy for different orientations and different degrees of anisotropy. In this section, we explain how the program is written and how it works.

We first restrict the domain for space variables to $[-5, 5]$ since the solution does not change when we extend the length size. Similarly we restrict the interval for time to $[0, 5]$ since we observe that the system reaches equilibrium at $t = 5$, i.e; the solutions are the same for $t \geq 5$. We use the stability criteria (3.8) and we pick $\Delta\zeta = 0.05$ and $\Delta t = 0.001$. For this purpose, we use 200 points for space variable and 5000 points for time variable. In order to simulate the orientation dependence profiles, the azimuthal angle θ, the polar angle ϕ, and degree of anisotropy ϵ^2, are used as input parameters. Next, by using equations (2.26), we obtain the components of the unit normal vector to the interface, n_x, n_y and n_z. By using these components, the program calculates the coefficients of the second derivatives; λ_x, λ_y and λ_z, with the help of (2.21). Then the code solves the system of equations by using the boundary and initial conditions for all order parameters.

Chapter 4

RESULTS

In the present chapter, we examine the behavior of the interface boundaries between the disordered phase and ordered phase at critical temperature. We perform the numerical calculation of the interface structures: First, we simulate the evaluation of order parameters, and then thickness of the interface as a function of orientation and time. Interfacial energy anisotropy of the IPPs is determined for different orientation and degree of anisotropy. We also add the convection term to the reaction-diffusion equation for [111] equation and simulate the effect of this term.

We use $\Delta\zeta = 0.05$, $\Delta t = 0.001$ and $\epsilon^2 = 0.005$ in our calculations and we observe no change after $t = 5$ second for equations of orientations [111], [110] and [100]; i.e the system reaches equilibrium at time $t = 5$.

4.1 Evolution of Order Parameters

For [111] orientation, computed solutions of the equation (2.28) are shown in Figure 4.1 and Figure 4.2. Figure 4.1 shows the one dimensional solution for order parameters. Due to the normal vector $\vec{n} = (\frac{1}{\sqrt{3}}, \frac{1}{\sqrt{3}}, \frac{1}{\sqrt{3}})$ and $\lambda_x^2 = \lambda_y^2 = \lambda_z^2 = \lambda^2 = \frac{1}{3}(1 + 2\epsilon^2)$, all order parameters are equal. As can be seen in this figure, thickness of interface is getting larger and the solution is getting smoother when the time evolves. The occupation densities are computed as a function of spatial variables and exhibited in Figure 4.2 for $t = 0.1$ and $t = 5$. This figure is also indicates how the thickness of the interface is changing with time. The case $\rho_1 = \rho_2 = \rho_3 = \rho_4$ corresponds to the disordered phase, and that of $\rho_1 \neq \rho_2 = \rho_3 = \rho_4$ corresponds to the ordered phase.

For [110] orientation, since $n_x = n_y = \frac{1}{\sqrt{2}}, n_z = 0$ and $\lambda_x^2 = \lambda_y^2 = \frac{1+\epsilon^2}{2}, \lambda_z^2 = \epsilon^2$, we have $X = Y$. The solution of the system (2.22) for [110] orientation is shown in Figure 4.3. The difference between X and Z is small due to the small relative sizes of derivative coefficient.

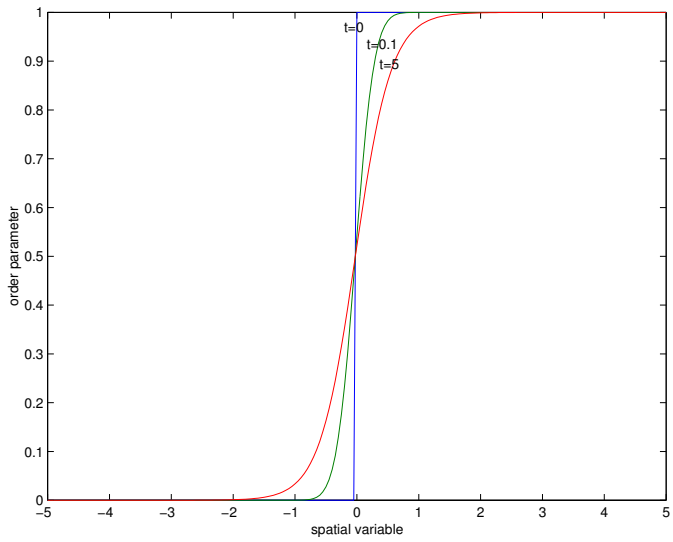

Figure 4.1: Evolution of order parameters for [111] orientation for seconds t= 0, t=0.1, t=5.

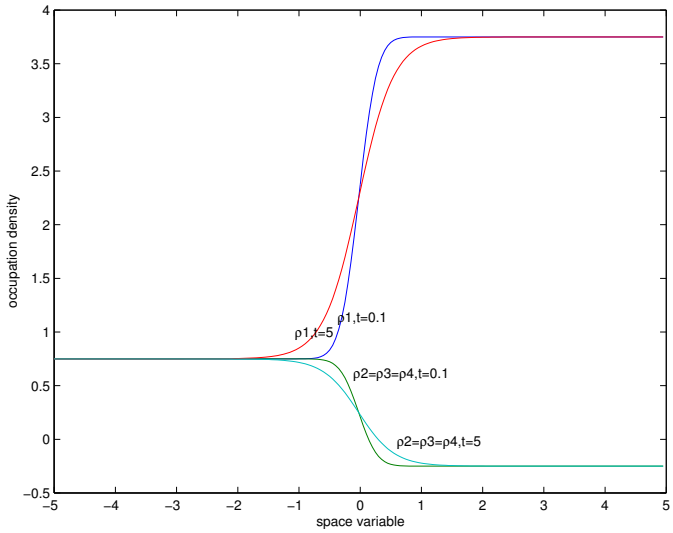

Figure 4.2: Changing of the occupation densities with respect to spatial variables for [111] orientation for seconds t=0.1 and t=5.

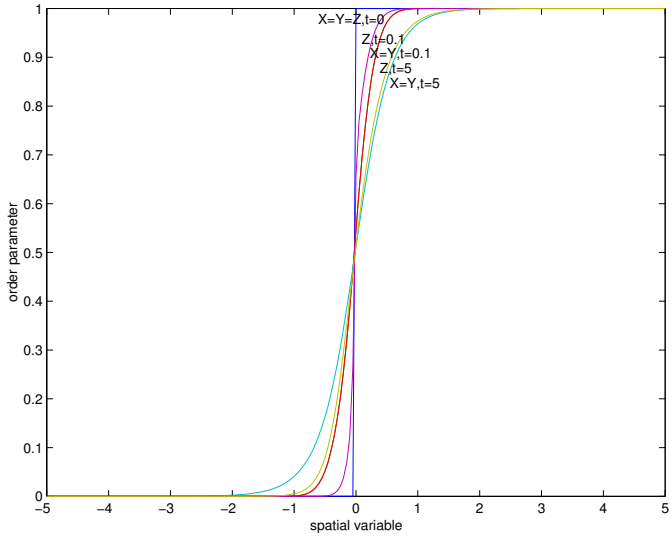

Figure 4.3: Evolution of order parameters for [110] orientation for seconds t= 0, t=0.1, t=5.

For an interface oriented in the [100] orientation, we have $n_x = 1, n_y = n_z = 0$ and $\lambda_x^2 = 1, \lambda_y^2 = \lambda_z^2 = \epsilon^2$. Computed order parameters are shown in the Figure 4.4. Because of the symmetries in the free energy functional, the behavior of the interface structures are the same for [001] and [010] orientations, therefore we only consider the [100] orientation. For those cases, any two of the order parameters are equal. Since the difference between the second derivative coefficients for [100] orientation is twice bigger than that of the [110] orientation, the separation between the order parameters for former orientation is larger than the latter one.

Finally, we compute the solutions of equation (2.22) for general orientation at critical temperature. The solution is shown in Figure 4.5 for azimuthal angle $\theta = 20°$ and polar angle $\phi = 40°$. All three non-conserved order parameters X, Y and Z are distinct for this case.

4.2 Thickness of Interface

The mathematical model, we are studying, assumes that there is a finite thickness of the interface because of the gradient term in the free energy of the system. We compute the thickness of the interface for different orientations and different degrees of anisotropy.

The computations are based on the following definition:

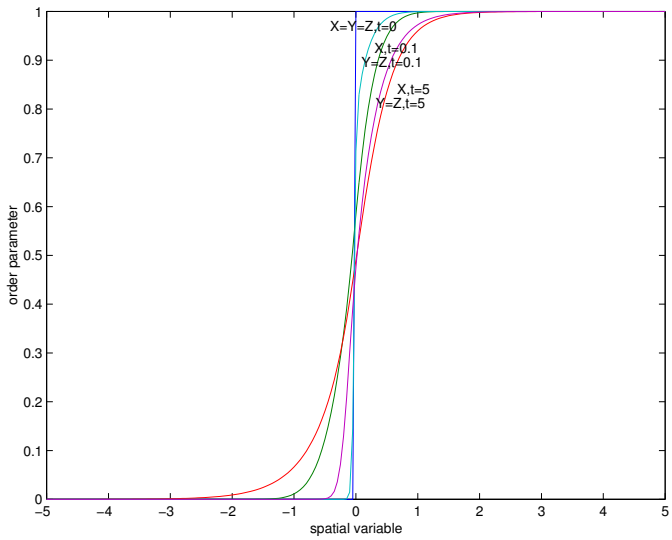

Figure 4.4: Evolution of the order parameters for [100] orientation for seconds t= 0, t=0.1, t=5.

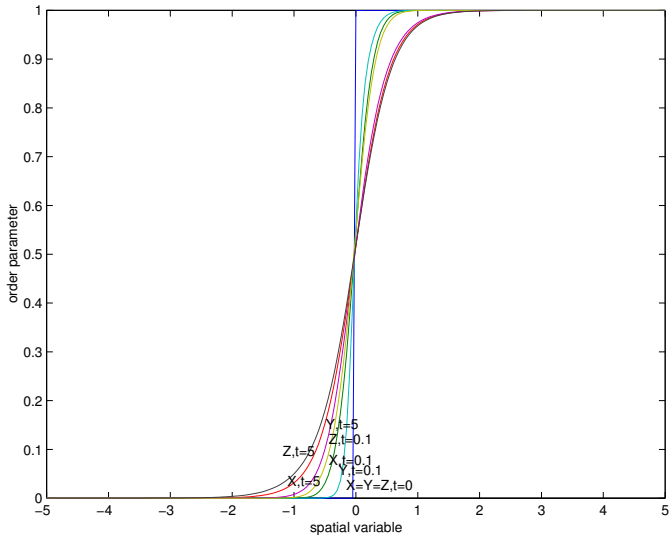

Figure 4.5: Evolution of the order parameters for $\theta = 20°$, and $\phi = 40°$ for seconds t= 0, t=0.1, t=5.

Definition 2.

Thickness of the interface at $t = t_0$ is the absolute value of the difference between the projection of the biggest left point (BLP) the smallest right point (SRP) on axis for spatial variable.

BLP is the point that satisfies the following conditions.

$$\sup_{X(a)}\{a \in [-L, L]\}, \text{ such that } X(a) = 0, \ X'(a) = 0 \tag{4.1}$$

and SRP is the point that satisfies

$$\inf_{X(a)}\{a \in [-L, L]\}, \text{ such that } X(a) = 1, \ X'(a) = 0. \tag{4.2}$$

The comparison of the thickness of interface for the orientations [111], [110], and [100] are exhibited in Figure 4.6 when the time evolves. As it can be seen, thickness of the interface is the largest in [111] orientation and the smallest for [100] orientation. This indicates that, it's approached to the edge of the spherical triangle, the thickness of the interface becomes smaller.

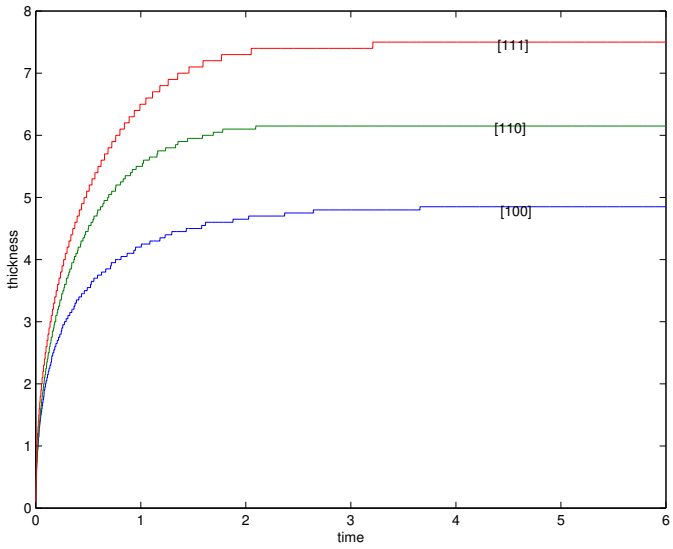

Figure 4.6: The changing of the thickness of the interface with time for different orientations.

The changing of the thickness of the interface with time for [100] orientation for different degrees of anisotropy is shown in Figure 4.7. As can be seen in this figure, the thickness of interface is proportional to degree of anisotropy.

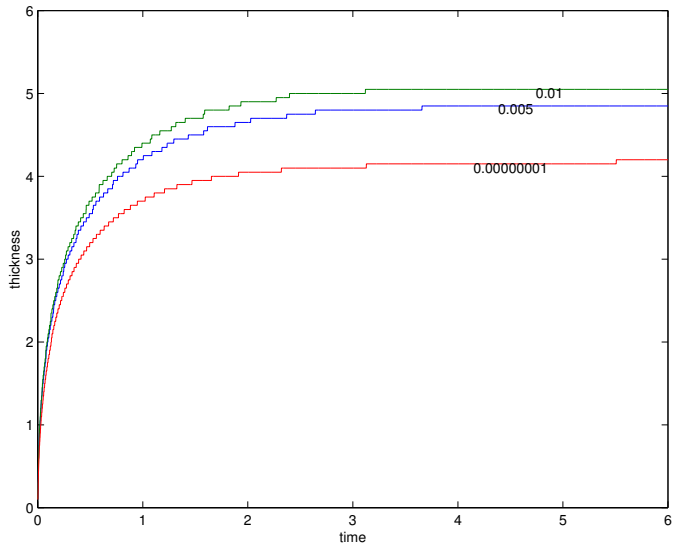

Figure 4.7: The changing of the thickness of the interface with time for [100] orientation for $\epsilon^2 = 10^{-2}$, $\epsilon^2 = 5.10^{-3}$, $\epsilon^2 = 10^{-8}$.

4.3 Interfacial Energy

After solving the system of equations (2.22) in terms of order parameters, we use the equation

$$\gamma = \int_{-5}^{5} \left\{ \lambda_x^2 X_\zeta^2 + \lambda_y^2 Y_\zeta^2 + \lambda_z^2 Z_\zeta^2 \right\} d\zeta, \tag{4.3}$$

to compute the interfacial energy γ which is a work that must be done at constant temperature and pressure to create unit area of the interface.

The integral that gives the interfacial energy is approximated by the trapezoidal rule from -5 to 5 by using the coefficients λ_x, λ_y, λ_z and calculating X_ζ, Y_ζ and Z_ζ.

Figure 4.8 shows the decaying profile for [100] orientation for $\epsilon^2 = 0.005$. This figure indicates that the transition between two states is so fast near critical temperature.

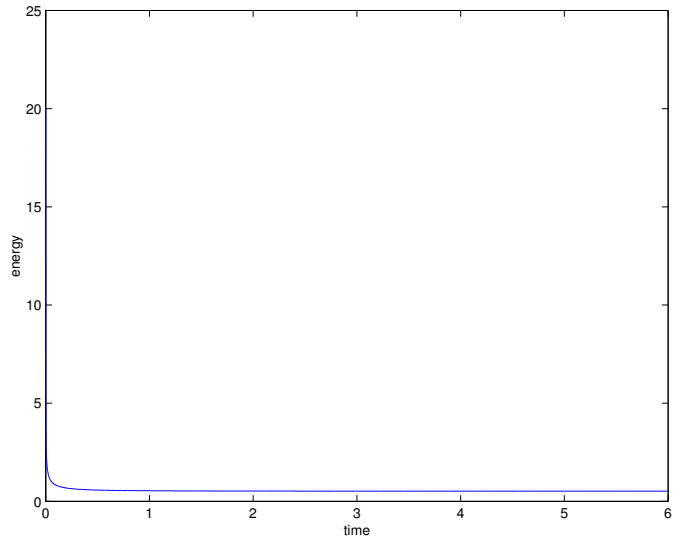

Figure 4.8: The changing of the interfacial energy with time for [100] orientation.

4.4 Solving the Problem with Different Initial Condition

In this section, we concern with the solutions of equations

$$X_t = \lambda^2 X_{\zeta\zeta} - 4a_2 X(X-1)(X-\frac{1}{2})$$

in Figure 4.9 for following initial condition

$$X(\zeta,0) = Y(\zeta,0) = Z(\zeta,0) = \begin{cases} 0 & \zeta \in [-L, \frac{-L}{3}) \\ \frac{1}{2} & \zeta \in [\frac{-L}{3}, \frac{L}{3}) \\ 1 & \zeta \in [\frac{L}{3}, L] \end{cases} \tag{4.4}$$

As is can be seen from the figure, the solution is bounded with the initial condition. Thus, the problem is well posed.

The solution imitates collision of two kinks (domain walls) (solitons) moving in opposite directions and creating one static kink.

It raises question if moving interface kink can be obtained as exact analytic solution and what is the velocity of this kink.

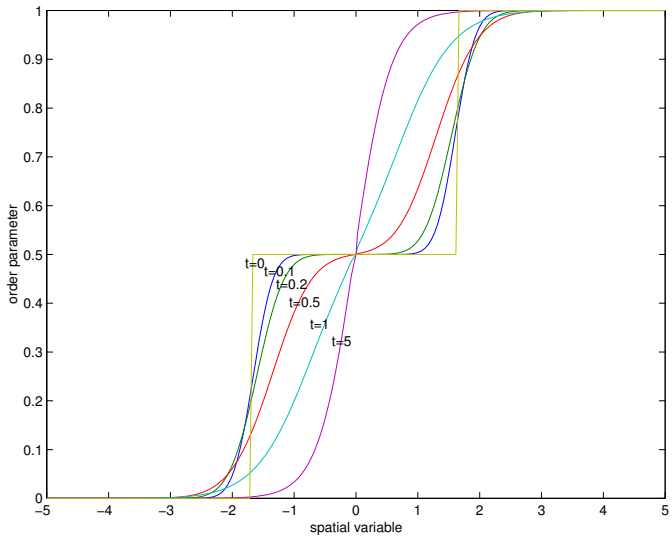

Figure 4.9: The solution of [111] equation for initial condition (4.4).

4.5 Relationship Between Three Simple Roots and the Wave Speed

To clarify these questions, in this section, we consider two types of non-linear reaction-diffusion equations

$$U_t = U_{xx} - (U - a_1)(U - a_2)(U - a_3) \tag{4.5}$$

and

$$U_t + \alpha U U_x = U_{xx} - \beta(U - a_1)(U - a_2)(U - a_3) \tag{4.6}$$

where a_1, a_2, a_3 are distinct real numbers; α and β are constants. The equation (4.5) has only non-linear reaction part and it is the generalization of dynamical [111] equation (2.28) for properly normalized function U, while the equation (4.6) has additional non-linear transport term. For both cases, the reaction part has the form of the third order polynomial which has three distinct roots. In the phase transition content, these three distinct roots correspond to the order of the system phases. From the phase plane analysis, the system has two stable and one unstable phases or one stable and two unstable phases. In the last case, no stable kink soliton can exist. The solutions of (4.5) and (4.6) give the connection between two stable phases correspond to the one soliton solutions. If solution of the problem is written with background value of one of the unstable phases, say a_3, then it gives the connection between two stable phases, a_1 and a_2. In the paper [41], one analytic soliton solution for the equations (4.5) and (4.6) are presented and also the relationship between three simple roots and the wave speed of the soliton for both equations is given. For equation (4.5), it's found that if one of

the roots is mean value of the other two roots, then the speed of soliton solutions is zero. For equation (4.6), it's shown that the restriction is removed on three distinct roots to obtain the non-stationary soliton by adding non-linear diffusion to the first equation by sketching the graphs of solutions [41]. The solution of equation (4.5) appears as travelling waves. The velocity of the waves is found as [41]

$$v = \pm \frac{a_1 + a_2 - 2a_3}{\sqrt{2}} \tag{4.7}$$

In Figure 4.10, the roots are considered as $a_1 = 0, a_2 = 1, a_3 = 0.5$ for equation (4.5). For this choice of roots, the velocity is of the soliton waves are calculated as $v = 0$. As it can be seen in this figure, there is no movement through either left or right.

On the other hand, when we consider the roots as $a_1 = 0, a_2 = 1, a_3 = 0.4$ for equation (4.5), it's seen that the velocity of the travelling wave is different from zero. The moving travelling wave solutions are exhibited in Figure 4.11 with the velocity $v = \frac{\sqrt{2}}{10}$.

For equation (4.6), the velocity of the waves is given by the formula as [41]

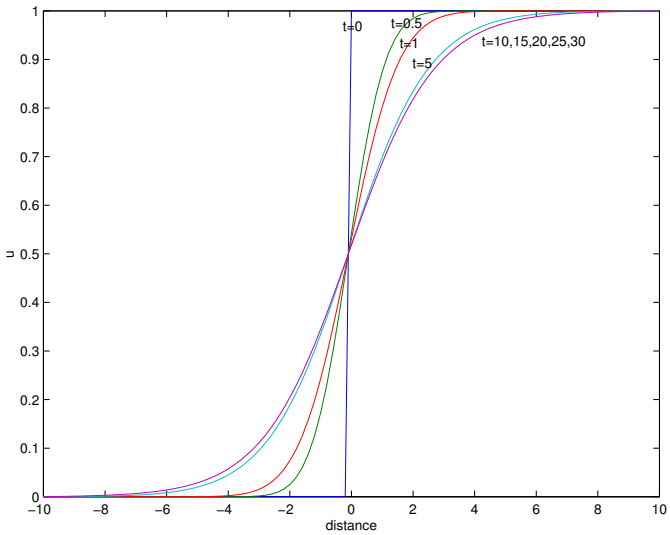

Figure 4.10: Evolution of the travelling wave with $v = 0$. The parameters are $a_1 = 0, a_2 = 1, a_3 = 0.5$.

$$v = \frac{2(a_1 + a_2 - 2a_3)}{\beta} - (\frac{a_2 + a_1}{2})\alpha \tag{4.8}$$

For simplicity, we pick $\alpha = \beta = 1$ in equation (4.6). Figure 4.12 shows that the velocity of the solution waves for equation (4.6) is different from zero as we expected from equation (4.8).

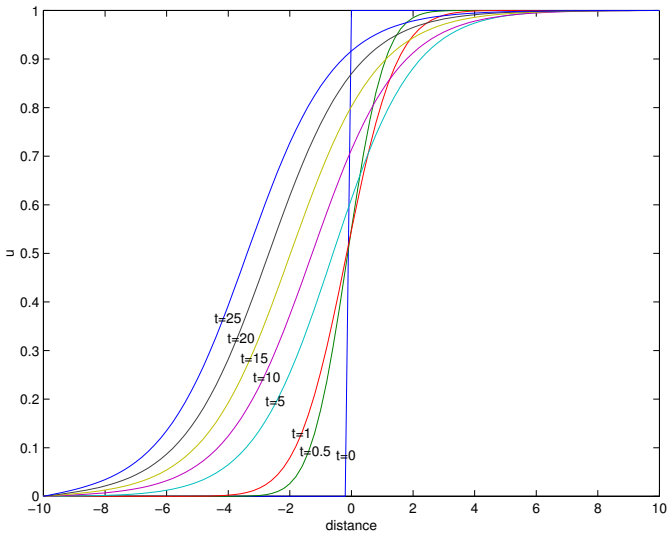

Figure 4.11: Evolution of the travelling wave with $v = \frac{\sqrt{2}}{10}$. The parameters $a_1 = 0, a_2 = 1, a_3 = 0.4$.

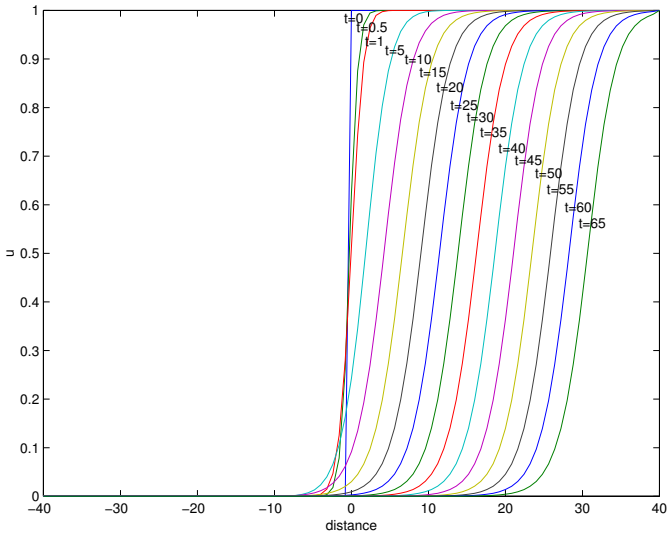

Figure 4.12: Evolution of the travelling wave with $v \neq 0$ for parameters $a_1 = 0$, $a_2 = 1$, $a_3 = 0.5$

Chapter 5

CONCLUSIONS

In this thesis, we extended the previous steady-state diffuse-interface model developed by Braun *et al* [16] to a non-steady-state problem. We then calculated the dynamics of microstructural changes for $Cu - Au$ alloys. We obtained the system of non-linear parabolic equations with the help of Langevin Equations. The finite differences method was implemented to solve the non-linear system of parabolic equations. The forward difference discretization was applied for the first derivative of the solution with respect to time and centered difference discretization was applied for the second order derivative of the solution with respect to spatial variable. Thus, order of convergence for the explicit finite difference is $O(\Delta t) + O((\Delta\zeta)^2)$. The stability criteria was also established to guarantee the convergence of the scheme. We also found the error bound for this scheme. The FORTRAN code was implemented and the package, MATLAB, was used for simulation.

First, we simulated the evolution of the order parameters for [111], [110] and [100] orientations. We found that the thickness of the interface is expanded as the time evolves. After very short time, the ordering process is ending. In order to see this result better, the thickness of the interface was simulated for [111], [110] and [100] orientations. We observed that the interface becomes thicker as the [111] orientation was approached. We also simulated the effect of the degree of anisotropy. For [100] orientation, we observed that thickness of the interface was getting narrower as the degree of anisotropy was getting smaller.

In order to see the speed of the process, we plotted graph of energy versus time. We found that ordering process is so fast for this system. We also showed the asymptotical stability. We plotted the exact solution of the equilibrium equation and the numerical solution of [111] equation at $t = 5$. We found that these two solutions are in a good agreement. Finally, we solve the system for [111] orientation by using different initial condition, and observed that the solution is

bounded with the initial condition. Thus, we saw that the problem is well-posed.

Our solutions exhibit the static travelling wave solution although we studied the dynamical model. We just observed the extension of the thickness of the interface when the time evolves.

Figure 5.1 shows the phase-plane for [111] equation. As can be seen in this figure, there are three equilibrium points, which are the solutions for this equation. Two stable points, $a_1 = 0$ and $a_2 = 1$, correspond to disordered and ordered phases respectively. Mathematically points of view, phase transition problem is considered as to find the minimum path to connect two stable points or disordered-ordered phases. The solution of this equation becomes a one-soliton-solution.

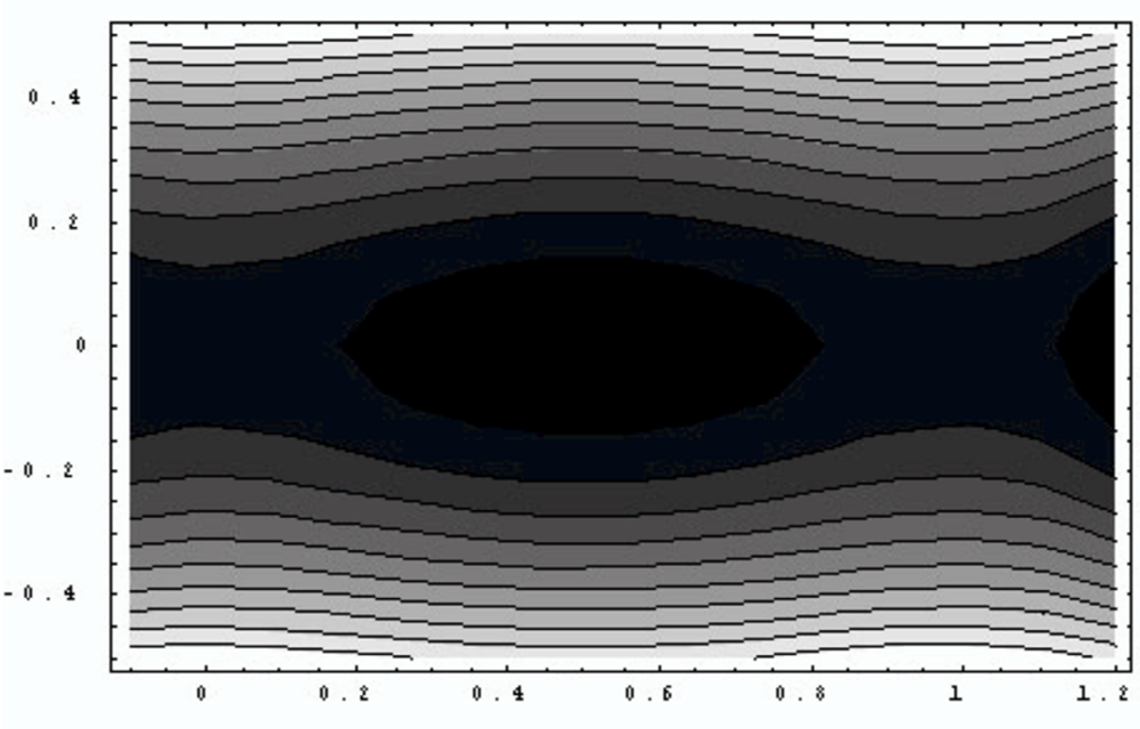

Figure 5.1: Phase plane for [111] equation.

Figure 5.2 shows the first derivative of the free energy functional. Since the total area is zero, the soliton solution does not move to the left or right. This result can be seen from the equation (4.7). In order to obtain travelling wave soliton, the transport term uu_x might be added to this equation.

In this study, we got more information about the ordering process for $Cu - Au$ system by extending the static problem to the non-stationary one. We believe that these information are very useful for the material scientists. The

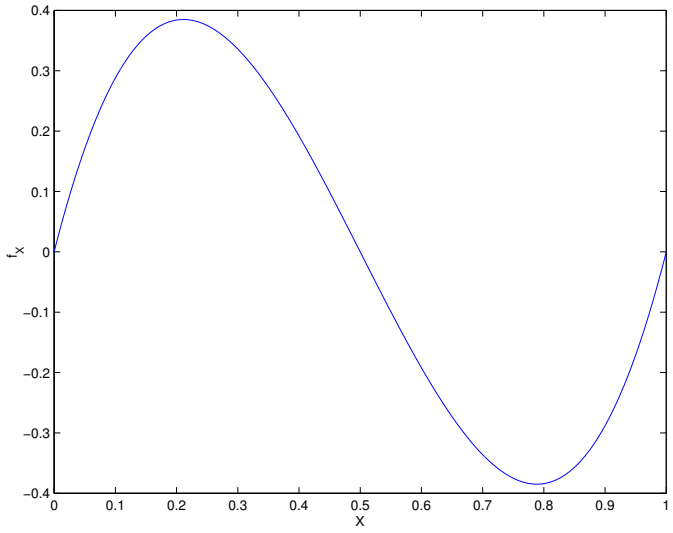

Figure 5.2: The graph of f_X.

phase field model is also very powerful to simulate the dynamics of microstructural changes in real alloys.

REFERENCES

[1] Van der Waals, originally published (in Dutch) in Verhandel. Konink. Akad. Weten. Amsterdam (Sect. 1), (1893), 1, 56: Translated by J.S. Rowlinson (in English) in J. Stat. Phys., 20, (1979), 197.

[2] Cahn J.W. and Hilliard J.E,. Acta metall. J. Chem. Phys. 28, (1958), 258.

[3] Allen S.M, and Cahn J.W,. Acta metall. 27, (1979), 1085.

[4] Ginzburg V.L., and Landau L.D,. J Exptl . Theoret. Phys. USSR. 20, (1950), 1064.

[5] Langer J.S., Directions in Condensed Matter, World Scientific, Singapore (1986).

[6] Caginalp, G., Phys. Rev. A 39, (1989), 5887.

[7] Kobayashi R.,. Physica D 63, (1993), 410.

[8] Wheeler A.A., Boettinger W.J., and McFadden G.B.,. Phys. Rev. A 45, (1992), 7424.

[9] Warren J.A., and Boettinger W.J., Acta metall. mater. 43, (1995), 689.

[10] Karma A., and Rappel, W.J., Phys. Rev. E 53, (1996)

[11] Wang S.L., and Sekerka R.F., Phys. Rev. E 53, (1996), 3760.

[12] Karma, A., and Rappel, W.J., Phys. Rev. E 57, (1998), 4323.

[13] Kim S.G., Kim W.T., and Suzuki, T. Phys. Rev. E 58, (1998), 3316.

[14] Kim S.G., Kim W.T., and Suzuki, Phys. Rev. E 60, (1999), 7186.

[15] Cha P.R, Yeon D.H, and Yoon J.K, A Phase Field Model for Isothermal Solidification of Multicomponent Alloys, Acta Materialia, 49, (2001), 3295-3307.

[16] Braun R. J., Cahn J. W., McFadden G. B., Wheeler A. A. Anisotropy of interfaces in an ordered alloy: A multiple-order-parameter model, Phil. Trans. R. Soc. Lond. A 355, (1997), 1787-1833.

[17] Allen, S.M., Cahn, J.W. A Microscopic Theory for Antiphase Boundary Motion and its Application to Antiphase Domain Coarsening. Acta metall. mater. 27, (1979), 1085-1095.

[18] Cahn, J.W. Allen, S.M. A microscopic theory for domain wall motion and its experimental verification in Fe-Al alloy domain growth kinetics. J. Phys. (Paris) Colloque, C7, (1977), 51-54.

[19] Cahn, J.W. On spinodal decomposition. Acta metall. 9, (1961), 795-801.

[20] Hilliard, J.E. Spinodal decomposition. In: Aaronson, H.I. (ed), Phase Transformations. American Society of Metals, Metals Park, OH (1970).

[21] Caginalp, G. Xie, W. Phase-field and sharp-interface alloy models. Phys. Rev. E 48, (1993), 1897-1909.

[22] Wheeler, A.A., Boettinger, W.J., McFadden, G.B. A phase-field model for isothermal phase transitions in binary alloys, Phys. Rev. A 45, (1992), 7424-7439.

[23] Wheeler, A.A., Boettinger, W.J., McFadden, G.B. A phase-field model of solute trapping during solidification, Phys. Rev. E 47, (1993), 1893-1909.

[24] Askeland, D. R., The Science and Engineering of Materials, (3 ed.) (1994). PWS Publishing Company, Boston, MA.

[25] Tanoğlu, G.B. Phase boundaries and anisotropy via multiple-order-parameter theory for an fcc alloy. Ph.D. University of Delaware, USA, (2000).

[26] Ansara, L., Sundman, B. and Wilemin, P. Acta Metall. Mater. 36, (1988), 977.

[27] Dupin, N. Contribution à l'évaluation thermodynamique des alliages polyconstitués à base de nickel. Ph. D. Thesis, Laboratoire de Thermodynamique et de Physico-Chimie Métallurgiques de Grenoble, Institute National Polytechnique de Grenoble. (1995)

[28] Tanoglu G., Braun R.J, Cahn J. and McFadden G.B. $A1 - L1_0$,Phase Boundaries and Anisotropy via Multiple - Order - Parameter Theory for an fcc Alloy, Interface and Free Boundaries, 5, (2003), 1-25.

[29] Novick-Cohen A., Cahn, J.W., Evolution Equations for Phase Separation and Ordering in Binary Alloys, J. Stat. Phys. 76, (1994), 877.

[30] Lifshitz, E.M, J. Physics, 6, (1942), 251-263.

[31] Krasnov M.L., Makarenko, G.I., Kiselev, A.I., Problems and Exercises in the Calculus of Variations, Mir Publishers, Moscow (1975), 80.

[32] Courant, R., Friedrichs, K. O., Lewy, H. Uber die partiellen Differenzengleichungen der Mathematischen Physik. Math. Ann. 100, (1928), 32-74.

[33] O'Brien, G. G., Hyman M. A., Kaplan S. A study of the numerical solution of partial differential equations. J. Math. Phy. 29, (1951), 223-251.

[34] John, F. On integration of parabolic equations by difference methods. Comm. Pure Appl. Math. 5, (1952), 155-211.

[35] Crank, J., Nicolson, P. A practical method for numerical integration of solution of partial differential equations of heat-conduction type. Proc. Cambridge Philos. Soc. 43, (1947), 50-67.

[36] Collatz, L. Numerische Behandlung von Differentialgbeichungen. Springer, Berlin, (1955)

[37] Forsythe, G. E., Wasow, W. R. Finite Difference Methods for Partial Differential Equations. Wiley, New York, (1960).

[38] Richtmyer, R.D., Morton, K.W. Difference Methods for Initial-Value Problems, Interscience, New York, (1967).

[39] Morton, K.W., Mayers, D.F Numerical Solution of Partial Differential Equations, Cambridge University Press, (1994), 52-53.

[40] Strikwerda, J.C., Finite Difference Schemes and Partial Differential Equations, Wadsworth and Brooks / Cole Advanced Books and Software, Pacific Grove, California (1989), 26.

[41] Pashaev O., Tanoğlu, G. The Hirota Method to Construct the Exact Solution of Reaction-Diffusion Equation which has Three Distinct Roots. (In progress)

APPENDIX

Here, the FORTRAN code we wrote to solve the system of equations and to obtain the data for simulation is given.

```
IMPLICIT DOUBLE PRECISION(A-H,O-Z)
DOUBLE PRECISION X(250),XL(6010),T(6010),
+U(250,6010),UP(250,6010),XR(6010),V(250,6010),
+VP(250,6010),W(250,6010),WP(250,6010),
+S(250,6010),SP(250,6010),ENER(6010)

OPEN(11,FILE='U.txt',STATUS='UNKNOWN')
OPEN(12,FILE='V.txt',STATUS='UNKNOWN')
OPEN(13,FILE='W.txt',STATUS='UNKNOWN')
OPEN(14,FILE='S.txt',STATUS='UNKNOWN')
OPEN(15,FILE='UP.txt',STATUS='UNKNOWN')
OPEN(16,FILE='VP.txt',STATUS='UNKNOWN')
OPEN(17,FILE='WP.txt',STATUS='UNKNOWN')
OPEN(18,FILE='XL.txt',STATUS='UNKNOWN')
OPEN(19,FILE='XR.txt',STATUS='UNKNOWN')
OPEN(20,FILE='DIFFERENCE.txt',STATUS='UNKNOWN')
OPEN(21,FILE='ENERGY.txt',STATUS='UNKNOWN')
OPEN(22,FILE='U1.txt',STATUS='UNKNOWN')
OPEN(23,FILE='U2.txt',STATUS='UNKNOWN')
OPEN(24,FILE='U4.txt',STATUS='UNKNOWN')
OPEN(25,FILE='V1.txt',STATUS='UNKNOWN')
OPEN(26,FILE='V2.txt',STATUS='UNKNOWN')
OPEN(27,FILE='V4.txt',STATUS='UNKNOWN')
OPEN(28,FILE='W1.txt',STATUS='UNKNOWN')
OPEN(29,FILE='W2.txt',STATUS='UNKNOWN')
OPEN(30,FILE='W4.txt',STATUS='UNKNOWN')

TOL=1.0D-5
PI = 4.0D0*ATAN(1.0D0)
A41=1.0D0
```

```
A2=2.0D0
A42=1.0D0
A3=-12.0D0
L=5.0D0
M=200.0D0
DX=(2.0D0*L) / DFLOAT(M)
DT=0.0010D0
T(1)=0.0D0
R=((6-T(1))/DT)+1
EPS=0.0050D0


WRITE(*,*) 'WRITE THETA'
READ(*,*) THETA
WRITE(*,*) 'WRITE PHI'
READ(*,*) PHI


TT = THETA * PI/180.0D0
P = PHI * PI/180.0D0


ANX = DSIN(P) * DCOS(TT)
ANY = DSIN(P) * DSIN(TT)
ANZ = DCOS(P)


EPSX = ANX**2 + EPS*ANY**2 +EPS*ANZ**2
EPSY = EPS*ANX**2 +ANY**2 + EPS*ANZ**2
EPSZ = EPS*ANX**2 + EPS*ANY**2 + ANZ**2


DO 10 N=1,R
U(1,N)=0
U(M+1,N)=1
V(1,N)=0
V(M+1,N)=1
W(1,N)=0
W(M+1,N)=1
 10 CONTINUE
```

```
DO 30 N=2,R
T(N)=T(1)+(N-1)*DT
 30 CONTINUE

X(1)=-L

DO 5 I=2,M+1
X(I)=X(1)+(I-1)*DX
 5 CONTINUE

DO 20 I=1,M+1
IF (X(I).LT.0.0D0) THEN
U(I,1)=0.0D0
V(I,1)=0.0D0
W(I,1)=0.0D0
ELSE
U(I,1)=1.0D0
V(I,1)=1.0D0
W(I,1)=1.0D0
ENDIF
 20 CONTINUE

DO 35 N=1,R-1
DO 40 I=2,M
U(I,N+1)=(U(I+1,N)-2*U(I,N)+U(I-1,N))*EPSX*
+DT/(DX*DX)-(2*A2*U(I,N)+A3*V(I,N)*W(I,N)+4*A41
+*U(I,N)*U(I,N)*U(I,N)+2*A42*U(I,N)*(V(I,N)*
+V(I,N)+W(I,N)*W(I,N)))*DT+U(I,N)

V(I,N+1)=(V(I+1,N)-2*V(I,N)+V(I-1,N))*EPSY*
+DT/(DX*DX)-(2*A2*V(I,N)+A3*U(I,N)*W(I,N)+4*A41
+*V(I,N)*V(I,N)*V(I,N)+2*A42*V(I,N)*(U(I,N)*
+U(I,N)+W(I,N)*W(I,N)))*DT+V(I,N)

W(I,N+1)=(W(I+1,N)-2*W(I,N)+W(I-1,N))*EPSZ*
```

```
+DT/(DX*DX)-(2*A2*W(I,N)+A3*U(I,N)*V(I,N)+4*A41
+*W(I,N)*W(I,N)*W(I,N)+2*A42*W(I,N)*(U(I,N)*
+U(I,N)+V(I,N)*V(I,N)))*DT+W(I,N)
 40 CONTINUE
 35 CONTINUE

DO 36 N=1,R
DO 38 I=1,M+1
IF ((EPSX.LE.EPSY).AND.(EPSX.LE.EPSZ)) THEN
S(I,N)=U(I,N)
ENDIF
IF ((EPSY.LE.EPSX).AND.(EPSY.LE.EPSZ)) THEN
S(I,N)=V(I,N)
ENDIF
IF ((EPSZ.LE.EPSX).AND.(EPSZ.LE.EPSY)) THEN
S(I,N)=W(I,N)
ENDIF
 38 CONTINUE
 36 CONTINUE

DO 42 N=1,R
DO 44 I=1,M
UP(I,N)=(U(I+1,N)-U(I,N))/DX
VP(I,N)=(V(I+1,N)-V(I,N))/DX
WP(I,N)=(W(I+1,N)-W(I,N))/DX
 44 CONTINUE
 42 CONTINUE

DO 50 N=1,R
DO 52 I=1,M
IF ((EPSX.LE.EPSY).AND.(EPSX.LE.EPSZ)) THEN
SP(I,N)=UP(I,N)
ENDIF
IF ((EPSY.LE.EPSX).AND.(EPSY.LE.EPSZ)) THEN
SP(I,N)=VP(I,N)
```

```
ENDIF
IF ((EPSZ.LE.EPSX).AND.(EPSZ.LE.EPSY)) THEN
SP(I,N)=WP(I,N)
ENDIF
 52 CONTINUE
 50 CONTINUE

DO 46 N=1,R
DO 47 I=1,M+1
IF (((SP(I+1,N).GT.TOL).AND.(SP(I,N).LT.TOL))) THEN
XL(N)=X(I)
WRITE(18,*) XL(N)
ENDIF
 47 CONTINUE
 46 CONTINUE

DO 58 N=1,R
DO 57 I=M+1,2,-1
IF (((SP(I,N).LT.TOL).AND.(SP(I-1,N).GT.TOL))) THEN
XR(N)=X(I)
WRITE(19,*) XR(N)
ENDIF
 57 CONTINUE
 58 CONTINUE

DO 65 N=1,R
WRITE(20,*) T(N),XR(N)-XL(N)
 65 CONTINUE

DO 80 N=1,R
ENER(N)=0
DO 81 I=2,M
ENER(N)=ENER(N)+((EPSX*UP(I,N)*UP(I,N))+(EPSY*
+VP(I,N)*VP(I,N))+(EPSZ*WP(I,N)*WP(I,N)))*DX
```

```
 81 CONTINUE
 80 CONTINUE

DO 82 N=1,R
WRITE(21,*) T(N),ENER(N)
 82 CONTINUE

DO 60 I=1,M+1
WRITE(22,*) X(I),U(I,1)
WRITE(23,*) X(I),U(I,101)
WRITE(24,*) X(I),U(I,5001)
WRITE(25,*) X(I),V(I,1)
WRITE(26,*) X(I),V(I,101)
WRITE(27,*) X(I),V(I,5001)
WRITE(28,*) X(I),W(I,1)
WRITE(29,*) X(I),W(I,101)
WRITE(30,*) X(I),W(I,5001)
 60 CONTINUE

STOP
END
```